

MATERIALS PERFORMANCE THRUST

Joe H. Payer, Materials Performance Thrust
Case Western Reserve University
Contact: 216.368.4218 | joe.payer@case.edu

Background

The Yucca Mountain site was recommended by the President to be a geological repository for commercial spent nuclear fuel and high-level radioactive waste. The site was then selected by Congress and signed into law by the President. The multi-barrier approach was adopted for assessing and predicting system behavior, including both natural barriers and engineered barriers. A major component of the long-term strategy for safe disposal of nuclear waste is to completely isolate the radionuclides in waste packages for long times. A further benefit is to greatly retard the egress and transport of radionuclides from penetrated packages. The goal of the Materials Performance Thrust program is to further enhance the understanding of the role of engineered barriers in waste isolation. In addition, the thrust will explore technical enhancements and seek to offer improvements in materials cost and reliability.

Opportunities for Performance and Technical Advances

The materials used for isolating waste in the proposed repository are an important component of the overall approach to the design of the repository system. The proposed emplacement drift is shown in Figure 1. Opportunities exist to enhance the understanding of material performance and to probe technical enhancements. These enhancements may include optimizing the performance of waste packages and drip shields for increased reliability and cost effectiveness.

Corrosion is a primary determinant of waste package performance at the proposed Yucca Mountain repository and will control the delay time for radionuclide transport from the waste package. Intact waste packages fully contain and isolate radionuclides at the proposed repository. Corrosion is the most likely degradation process that will determine when packages will be penetrated and also the shape, size, and distribution of those penetrations. Thus, corrosion resistance is important to the long-term performance of waste packages. This thrust program strives for increased scientific understanding, enhanced process models, and advanced technologies for long-term corrosion performance. The waste packages are manufactured from highly corrosion-resistant metals, and the surface of these metals is protected by the formation of a self-healing, passive layer. The metals for waste packages and drip shields have excellent corrosion resistance over a wide range of aqueous solution compositions and temperatures. Based upon measurements of corrosion rates of passive metals, if the passive film remains stable, the waste packages can remain

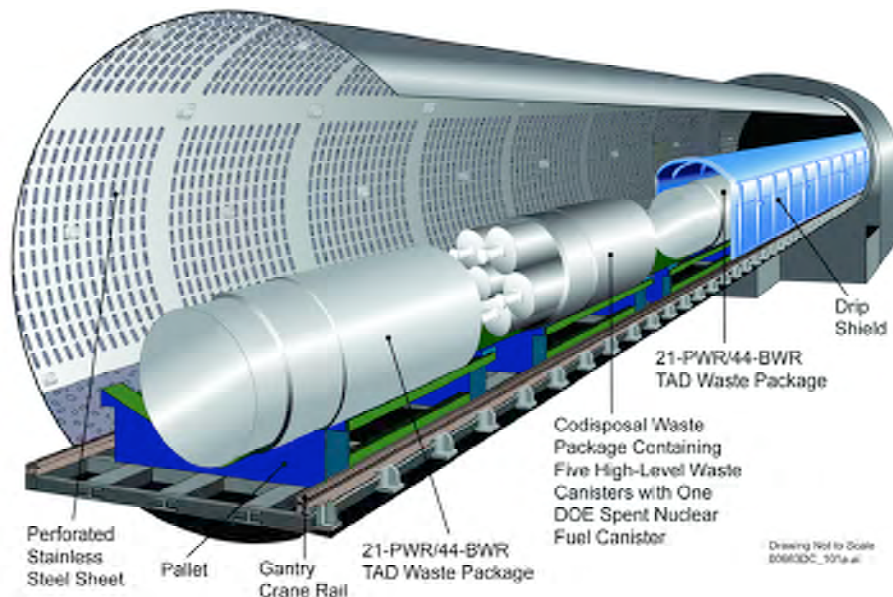


Figure 1. Proposed emplacement drift.

intact with no penetrations resulting from corrosion for durations of tens of thousands and even hundreds of thousands of years.

Materials Performance Thrust Program Team

A team of experts from universities was formed by the DOE Science and Technology program under a Corrosion Cooperative (CorrCoOp). This team works closely with scientists and engineers at several national laboratories and other participants. The CorrCoOp is based at Case Western Reserve University and includes investigators at Arizona State University, Case Western Reserve University, Ohio State University, Pennsylvania State University, University of California-Berkeley, University of Minnesota, University of Toronto, University of Western Ontario, and University of Virginia. National laboratories that have participated include Argonne National Laboratory (ANL), Lawrence Livermore National Laboratory (LLNL), Lawrence Berkeley National Laboratory (LBNL), Oak Ridge National Laboratory (ORNL), Pacific Northwest National Laboratory (PNNL) and Sandia National Laboratories. Other participants include Atomic Energy of Canada Limited (AECL)

and OLI Systems Inc. A sampling of the specialized capabilities and facilities is shown in Figure 2.

Targeted Technical Thrusts

There are three multi-investigator projects within the Materials Performance Thrust. Each of these is a coordinated set of collaborative efforts.

Corrosion of Metal Surfaces Covered with Particulate and Deposits

The waste packages are supported in air, and they will never be fully immersed in water. Rather, the metal surfaces may be covered with dust, particulate, and moisture from the surrounding rock and humidity. The analysis of corrosion cells under these conditions is a primary objective.

Evolution of Corrosion Damage by Localized Corrosion

Understanding of localized corrosion processes, and particularly crevice corrosion, is a high priority. The examination of the rate of penetration and extent of corrosion damage by factors that determine localized corrosion over extremely long times is important.

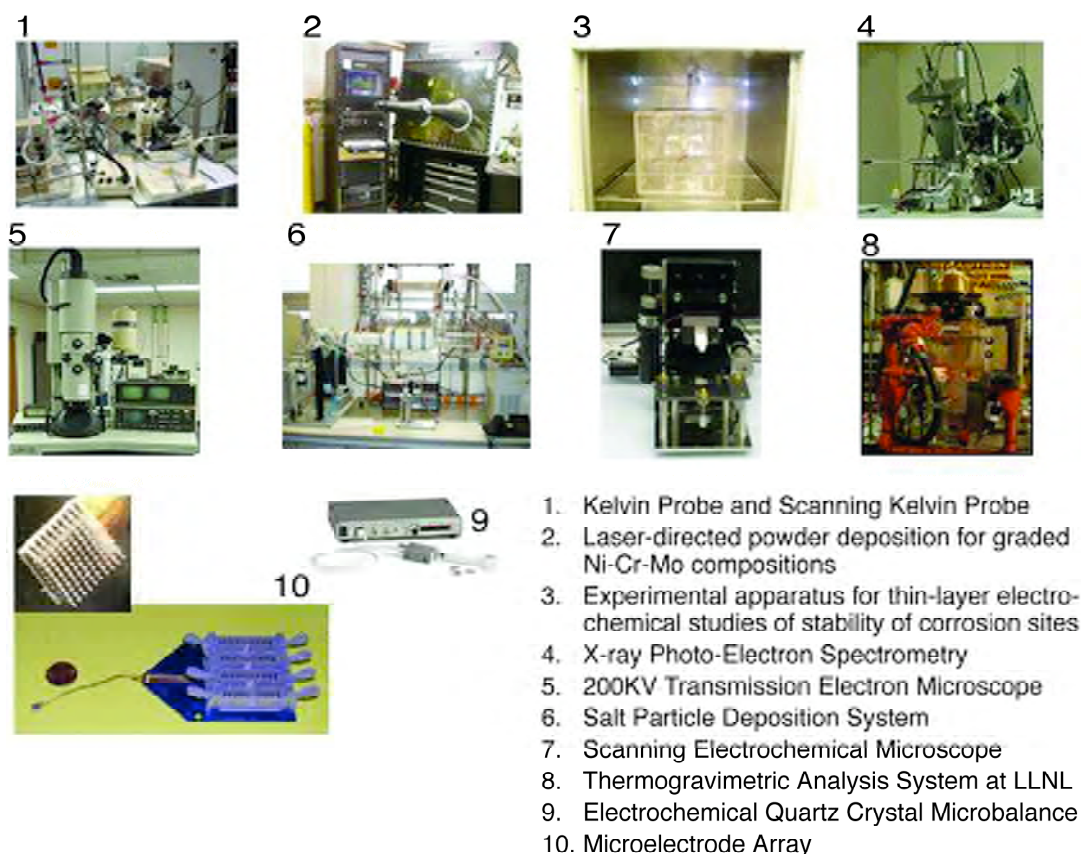


Figure 2. Sampling of the specialized capabilities and facilities of the Corrosion Cooperative.

Evolution of Moisture Environment on Metal Surfaces

The corrosion performance of a metal is determined by the inherent corrosion resistance of the metal and the corrosivity of the environment to which the metal is exposed. The amount, distribution, and chemical composition of the moisture on waste packages are primary determinants of corrosion performance.

In addition to the multi-investigator projects, there are bridging projects that coordinate and integrate process-modeling activities in the Materials Performance Thrust to those in the Natural Barriers Thrust and the Source Term Thrust. The Materials Performance Thrust has been an incubator for work that transitioned to full development projects under the Advanced Technologies Thrust, e.g., advanced welding techniques and high-performance amorphous metal coatings.

Corrosion of Metal Surfaces Covered with Particulate and Deposits

The objective of this multi-investigator effort is to determine the corrosion behavior of corrosion-resistant metal surfaces that are covered by thin layers of moisture and moist particulate and deposits. Advanced analytical and computational methods for corrosion processes in thin films, particulates, and deposits are developed. Inputs are generated for advanced, next-generation models and alternate conceptual models, based on less conservative assumptions. Enhanced scientific understanding of chemical, electrochemical, and corrosion processes is provided.

Targeted thrust objective: *Develop technical basis for and demonstrate the reduction in passive corrosion rate with time. There is a potential to extend predicted waste package life by 100 to 1,000 times compared to that predicted using a time-invariant rate.*

Highly corrosion-resistant materials are selected for the waste packages and drip shields for the proposed Yucca Mountain repository, i.e., Alloy 22, a nickel-chromium-molybdenum (Ni-Cr-Mo) alloy, and titanium (Ti), respectively. In oxidizing environments that are of interest for the proposed repository, these alloys depend upon the formation and the tenacity of a passive film, i.e., a thin oxide on the metal surface, for their corrosion resistance. Measured corrosion rates for passive metals decrease with time to (on the order of) 0.1 to 0.01 micrometer per year. At these rates, it takes 10,000 to 100,000 years to penetrate 1 mm of metal, and the Alloy 22 outer layer of the waste packages is on the order of 20 mm thick. Thus, accounting for the reduction in passive corrosion rates is important to life prediction.

Targeted thrust objective: *Identify corrosion processes for*

metal covered with particulate and deposits. Where corrosion is based on fully immersed solutions and not corrosion in moist layers of dust/particulate, the fully immersed treatment is conservative in many cases.

In the proposed repository, metal surfaces will be dry (no corrosion) in contact with thin layers of moisture or moist particulates or deposits. The waste packages are placed on support pallets and sit in air at atmospheric pressure. There is no feasible scenario that will lead to waste packages being fully immersed in water. There is a limited amount of water moving through the rock, and there is a limited amount of salts and minerals available to deposit on the packages. The ambient waters in the mountain are dilute; however, those ambient waters can be modified and become concentrated by thermal-hydrological-chemical processes. The sources of water that can contact metal surfaces in the proposed repository are deliquescence, condensation and drips or seepage. Deliquescence (to dissolve and become liquid by absorbing moisture from the air) is determined by the composition of soluble salts in the particulate layers, the relative humidity, and temperature. Drips and seepage of water from the drift walls onto the metal surfaces are possible after the thermal barrier period, i.e., when the drift wall has cooled to below the boiling point of water. Metals will be exposed to thin layers of moisture and moist particles in deposits of dust and particulate.

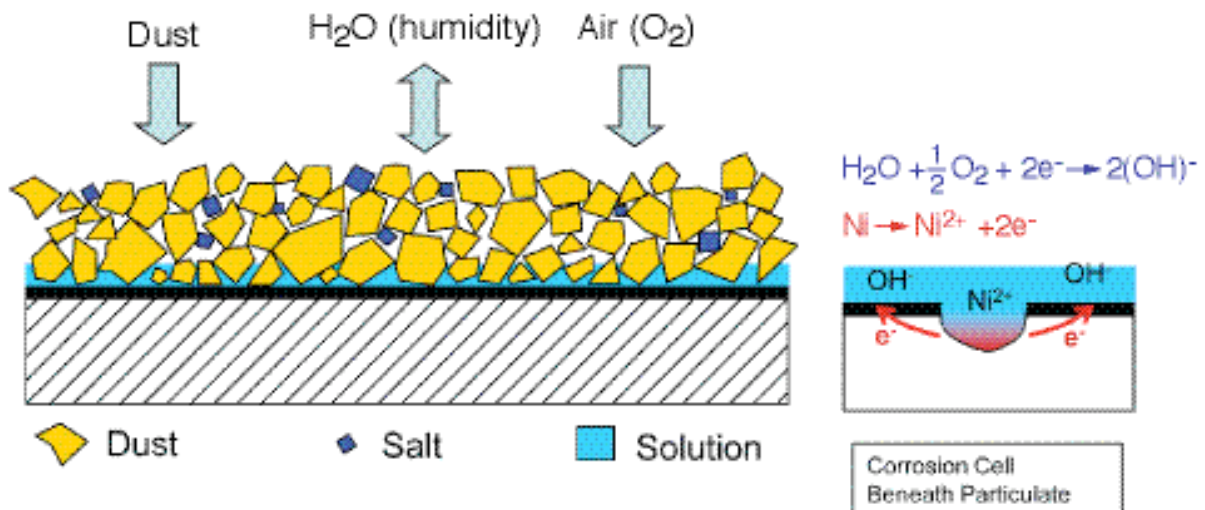
A schematic diagram of corrosion in thin layers of particulate and a list of important parameters that affect corrosion are presented in Figure 3.

Significant progress has been made in the following tasks:

- Analysis of passive film properties and changes in corrosion rate with time
- Analysis of the role of oxygen reduction rates on corrosion and passivity
- Coordination of computational modeling and experimental projects
- Development and implementation of specialized experimental methods for corrosion and electrochemistry in thin layers of particulate and moisture
- Determination of relationships between the structure and composition of the passive film and the corrosion resistance of Ni-Cr-Mo alloys
- Elucidation of the corrosion processes in thin films, particulate, and deposits

The S&T Materials Performance funded projects related to Corrosion of Metal Surfaces Covered with Particulate and Deposits (pp. 63-76) are:

- “Kinetics of the Cathodic Reduction of Oxygen on



- Dust deposited
- Degree of wetness
- Soluble salts
- Gas composition and property, T, RH
- Particulate layer properties, such as conductivity, temperature, pH, degree of wetness, etc.
- Localized environment on the surface
- Anode: $\text{Ni} \rightarrow \text{Ni}^{2+} + 2\text{e}^-$
- Cathode: $\text{H}_2\text{O} + 1/2\text{O}_2 + 2\text{e}^- \rightarrow 2\text{OH}^-$

Figure 3. Schematic diagrams of corrosion of a metal covered by a thin layer of particulate and a corrosion cell beneath the particulate.

- “Passive Metals” by Shoesmith et al.
- “Oxygen Electro-Reduction on Passive Metals” by Gervasio et al.
- “Corrosion Cells beneath Thin Films, Particulate and Deposited Layers” by Payer et al.
- “Electrochemical Measurements of Corrosion under Thin Brine Layers” by Frankel et al.
- “Mechanism of Mixed-Ion Effects on Corrosion in Thin Films” by Newman et al.
- “Effect of Environmental Variables on the Structure and Composition of Passive Films” by Devine et al.

Evolution of Corrosion Damage by Localized Corrosion

Localized corrosion processes and particularly crevice corrosion are high priorities. This technical thrust examines the rate of penetration and extent of corrosion damage by localized corrosion over extremely long times. Advanced analytical and computational methods for the time evolution of crevice-corrosion damage are developed. The requirements for the initiation and propagation of localized corrosion are determined. In addition, a focus is on the phenomena and processes that can result in the reduction in the rate, or complete arrest, of crevice corrosion.

Targeted thrust objective: Develop and analyze a logic-tree approach for the damage to waste packages by localized corrosion. In contrast to a simple go/no-go initiation criterion, the logic-tree approach provides a clear and transparent treatment to account for contributing factors.

Targeted thrust objective: Develop the technical basis for and demonstrate processes that slow penetration rates by localized corrosion in contrast to a treatment where a constant rate is presumed once damage (crevice corrosion) is started and there is no slowing or stopping of penetration rate. Where processes of stalling (slower rates) and arrest (corrosion stops) pertain, the amount of damage over long periods of time would be greatly reduced.

Targeted thrust objective: Demonstrate factors that may limit the initiation and propagation of localized corrosion. In contrast to a treatment that presumes crevices and supporting processes are always available, examine localized corrosion processes simulating coverage by rock and particulate.

The evolution of crevice-corrosion damage is determined by the initiation, propagation, stalling, and arrest stages of this form of localized corrosion. Crevice corrosion is affected by the crevice geometry and properties of the crevice former. For waste packages, metal surfaces can be covered with dust and particulate. The particulate, scale, and

deposits can form from dust, minerals from waters, and corrosion products. An important issue is how effective particulate layers and deposits are as crevice formers compared to metal/metal crevices on waste packages and polymer/metal crevices used in laboratory tests. Chemical, electrochemical, and metallurgical factors control the formation and evolution of the crevice solution chemistry. For crevice corrosion to persist, a critical crevice solution chemistry must be formed and maintained within the occluded region. These and other crucial issues are addressed by the projects in this technical thrust area.

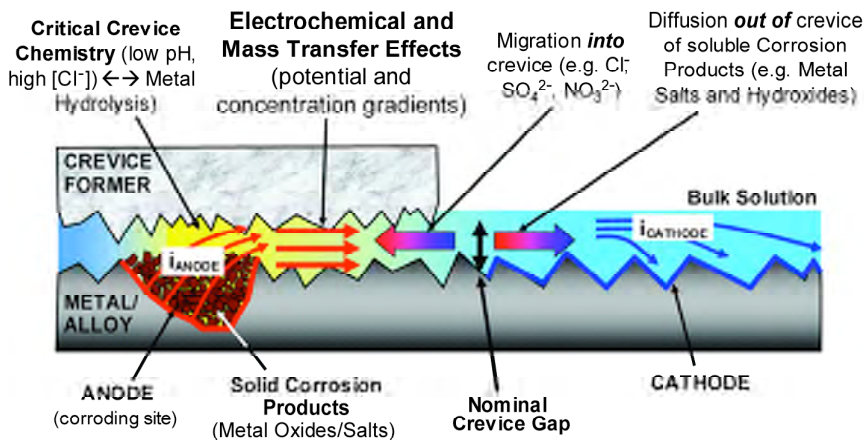


Figure 4. Schematic diagram of processes during crevice corrosion.

The approach has been to meet the objectives through a coordinated set of projects. Examples of the experimental methods and analytical modeling in this area are shown in Figures 4 and 5.

Significant progress has been made in the following tasks:

- Development and analysis of a logic-tree approach for the damage by localized corrosion
- Identification of the role of the interrelationship among anodic, cathodic, and coupled processes in the determination of crevice-corrosion behavior
- Coordination of computational modeling and experimental projects
- Development and implementation of specialized experimental methods for crevice-corrosion initiation, propagation and arrest
- Determination of the relationships between metallurgy (corrosion resistance of metals) and water chemistry (corrosivity of the environment) for Ni-Cr-Mo alloys and less corrosion-resistant metals in high-temperature, multi-species waters
- Establishment of a framework and process for the incorporation of findings into advanced methods for the “Prediction of Time Evolution of Localized Corrosion Damage”

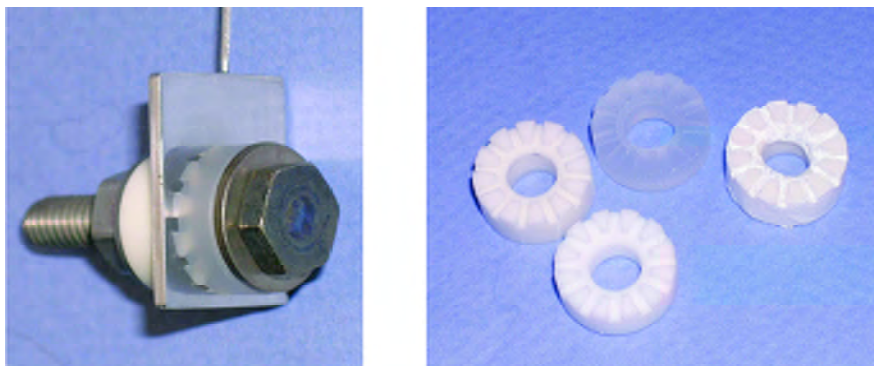


Figure 5. A multicrevice test assembly and crevice formers made from polymers and ceramics.

Corrosion” by Kelly et al.

- “Crevice-Corrosion Damage Function on Alloy-22” by Shoesmith et al.
- “Localized Corrosion Stability in the Presence of Non-Chloride Anions” by Newman et al.
- “Metallurgical Effects on Localized Corrosion of Ni-Cr-Mo Alloys” by Frankel et al.
- “Processes in Crevice-Corrosion Propagation, Stifling, and Arrest” by Payer et al.
- “Combinatorial Chemistry Approaches for Alloy Composition and Corrosion Behavior” by Buchheit et al.
- “Prediction of the Time Evolution of Localized Corrosion Damage” by Macdonald et al.

Evolution of the Moist Environment on Metal Surfaces

The S&T Materials Performance funded projects related to Evolution of Corrosion Damage by Localized Corrosion (pp. 77-94) are:

- “Crevice-Corrosion Electrochemistry of Ni-Cr-Mo Alloys” by Scully et al.
- “Modeling of Critical Chemistry for Crevice

The corrosion performance of a metal is determined by the inherent corrosion resistance of the metal and the corrosivity of the environment. The amount, distribution, and chemical composition of the moisture on waste packages are controlling parameters of corrosion performance. The

objective is to determine the properties of thin layers of moisture, moist particulates, and deposits that will affect the corrosion performance of metals. Advanced analytical and computational methods for the evolution of the environment on metal surfaces are developed. Scientific understanding is enhanced for moisture formation, chemistry, and evolution with time and for the properties of thin layers of particulates and deposits on metal surfaces.

Targeted thrust objective: *Develop and demonstrate evolution of environment (moisture) on metal surfaces in layers of moisture, particulate, and deposits.*

Key issues for corrosion behavior and long-term performance are determination of the presence of moisture on metal surfaces, the corrosive properties of the moisture, and the corrosion resistance of materials in these environments. Thin layers of electrolyte, particulates, and deposits are the conditions of interest for the analysis of corrosion of waste packages. A special feature of the proposed Yucca Mountain repository is the extremely long time frame of interest. Thus, the time evolution of the environment in contact with waste package surfaces and the time evolution of corrosion damage that may result are of primary interest in the determination of expected performance.

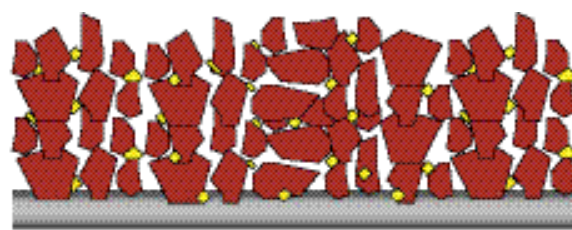
In the proposed repository, moisture can form on the metal surfaces by deliquescence and condensation processes as the waste packages cool from high temperatures after the heat-up period. A thermal barrier prevents drips and seepage into the drifts as long as the drift wall is hotter than the boiling point of water. After the thermal barrier period, a source of moisture on the metal surfaces is drips or seepage from the rock formation onto waste packages.

It is well accepted that dry metals, without the presence of an aqueous phase, do not corrode at an appreciable rate. Furthermore, full immersion in waters will not occur at the proposed repository under any realistic scenario. Therefore, corrosion in thin layers of electrolyte, particulate, and deposits are the conditions of interest. These thin layers of moisture can be a sufficient aqueous environment to support electrochemical dissolution. Anodes, cathodes, and an electrochemical corrosion cell can operate in a thin moisture layer. However, the factors that determine the onset of corrosion and the subsequent degree of damage can vary significantly in thin layers compared to fully immersed conditions.

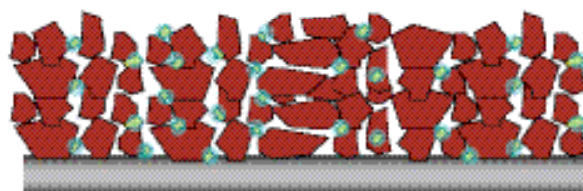
The approach has been to meet the objective through a coordinated set of projects. Figure 6 shows several scenarios for the distribution of moisture within a layer of particulates.

Significant progress has been made in the following tasks:

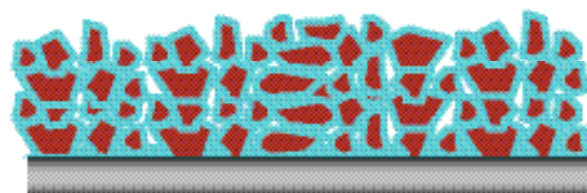
- Coordination of experimental and computational



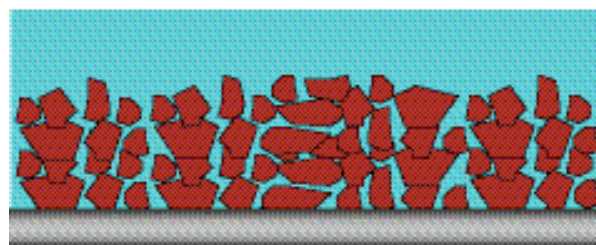
(a) Dry particulate – No moisture



(b) Droplets of moisture



(c) Unsaturated particulate layer



(d) Solution layer on metal

Figure 6. Scenarios for the distribution of moisture in a particulate layer.

projects to examine corrosion current distributions in moist particulate layers on metal surfaces.

- Determination of the properties and behavior of high-temperature multispecies solutions.
- Combination of the expertise and specialized facilities in geochemistry, corrosion, electrochemistry, and materials science.
- Establishment of a framework and process for incorporation of findings into advanced methods for the "Prediction of Time Evolution of Localized Corrosion Damage."
- Development and application of advanced analytical methods and sensors to determine the

properties of layers of moisture and particulate on metal surfaces.

The S&T Materials Performance funded projects related to Evolution of Environment on Metal Surfaces (pp. 95-108) are:

- “Modeling Chemical Environments within Corroding Crevices for Ni-Cr-Mo Alloys” by Wang et al.
- “Evolution of Solution Layer Chemistry during Localized Corrosion” by Kelly et al.
- “Modeling and Measurement of Current

Distribution on Particulate and Deposited Layers” by Landau et al.

- “Microelectronic and MEMS Devices for Solution Properties and Corrosion Evaluations” by Liu et al.
- “Optical Probes and Sensors to Determine Concentration Distributions in Thin Films on Reactive Surfaces” by Smyrl et al.
- “High-Temperature, Multi-Species Solution Properties and Behavior” by Cole et al.

Descriptions of projects in the Materials Performance Thrust area are provided in the following pages.

This page intentionally left blank.

CORROSION OF METAL SURFACES COVERED WITH PARTICULATE AND DEPOSITS

Kinetics of the Cathodic Reduction of Oxygen on Passive Metals

David W. Shoesmith, Dmitrij Zagidulin, Xueyuan Zhang, and James J. Noël,
University of Western Ontario

Oxygen Electro-Reduction on Passive Metals

Dominic Gervasio and Stephen P. Rogers, Arizona State University

Corrosion Cells Beneath Thin Films, Particulate, and Deposited Layers

Joe H. Payer, Pallavi Pharkya, Xi Shan, Arun S. Agarwal, and Hongyi Yuan
Case Western Reserve University

Electrochemical Measurements of Corrosion under Thin Brine Layers

Gerald S. Frankel, Rudolph G. Buchheit, Bastian Meier, and Shoichiro Taira,
Ohio State University

Mechanism of Mixed-Ion Effects on Corrosion in Thin Films

Roger C. Newman and Christopher Healey, University of Toronto

Effect of Environmental Variables on the Structure and Composition of Passive Films

Thomas M. Devine, Tzipi Cohen-Hyams, Marcela Miyagusuku, and Scott Harrington,
University of California, Berkeley

This page intentionally left blank.

Kinetics of the Cathodic Reduction of Oxygen on Passive Metals

David W. Shoesmith, Dmitriy Zagidulin, Xueyuan Zhang, and James J. Noël
University of Western Ontario

Research Objectives

The primary goal of this project is an elucidation of the mechanism and kinetics of the cathodic reduction of oxygen on Alloy 22, a nickel-chromium-molybdenum (tungsten) alloy. The accumulation of damage can be controlled either anodically (i.e., by the oxidative dissolution of the alloy components) or cathodically (i.e., by oxygen reduction). A clear definition of which of these two possible reactions is rate controlling, and a quantitative specification of the reaction kinetics, is important to the conceptual and numerical development of a corrosion model.

Approach

To characterize the electrical properties of the thin passive oxide formed on the alloy surface, EIS (Electrochemical Impedance Spectroscopy) experiments have been conducted on Alloy 22 in deaerated 5 mol/L NaCl solutions at different temperatures. The data obtained have been analyzed using different electrical equivalent circuits.

Note: all potentials are indicated with respect to the saturated Ag/AgCl electrode, $E=199$ mV vs. SHE.

Cyclic voltammetry (CV) experiments have been run in order to determine the electrochemical activity of the alloy surface preoxidized at different potentials and temperatures.

The electrochemical data have been correlated with the oxide composition and structure determined from XPS (X-ray Photoelectron Spectroscopy) and ToF SIMS (Time of Flight Secondary Ions Mass Spectrometry) experiments on Alloy 22 at different conditions in a deaerated 5 mol/L NaCl solution.

Accomplishments

From XPS and ToF SIMS data, it is clear that the protective film has a layered structure (Figure 1). Cr(III) and Ni(II) hydroxides, Mo(VI) and W(VI) oxides form the outer layer. Ni(II) and Cr(III) oxides, Mo(II), Mo(IV), and non-stoichiometric Mo

oxides constitute the inner layer. Also, XPS data show that the relative concentration of Cr_2O_3 is at a maximum for preoxidation potentials (E_{pox}) in the range 0 to 0.2 V. At more positive E_{pox} , this Cr(III) oxide is partially converted to CrO_4^{2-} (soluble) and $\text{Cr}(\text{OH})_3$. At the same potentials conversion of Mo^{2+} and Mo^{4+} to Mo^{6+} takes place, and

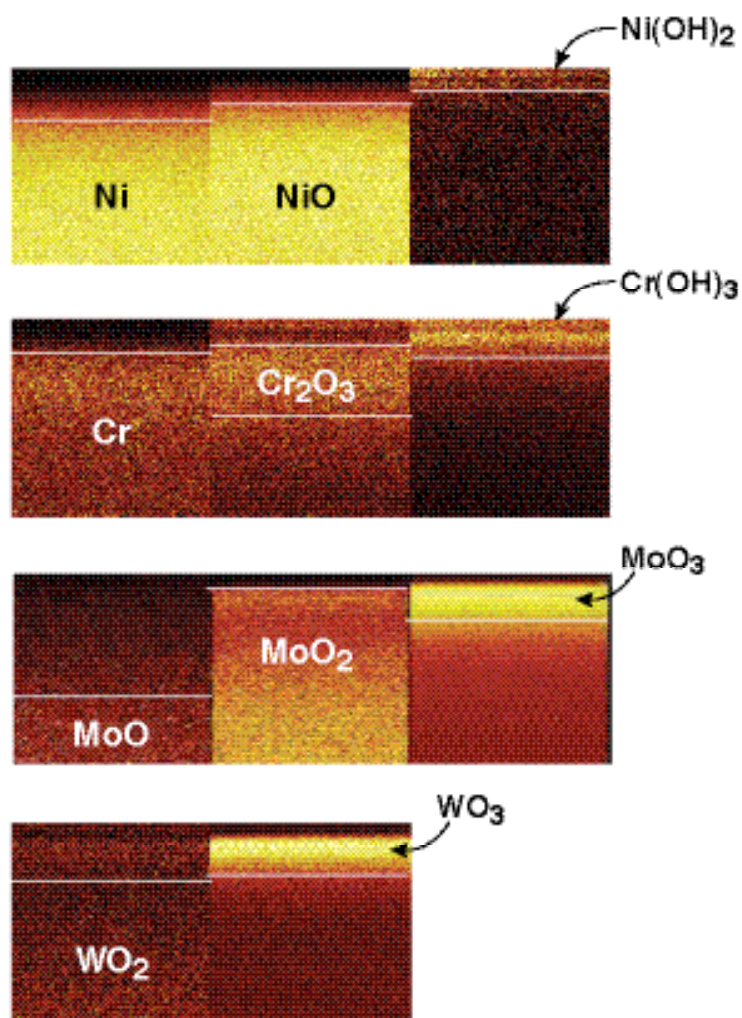


Figure 1. ToF SIMS depth profile obtained on Alloy 22. The oxide film was formed at 30°C and $E_{\text{pox}} = 0$ V. First row—Ni, NiO, Ni(OH)₂; second row—Cr, Cr₂O₃, Cr(OH)₃; third row—MoO, MoO₂, MoO₃; fourth row—WO₂, WO₃. The film/solution interface is on the top of each profile.

MoO₃ becomes the dominant Mo compound. Those changes coincide with a decrease in the film resistance (established by EIS) and create conditions where the surface can support oxygen reduction.

EIS data can be modeled taking into account three main processes, charge transfer through alloy/film interface; charge migration and diffusion in the oxide; and charge transfer at the oxide/solution interface. Charge transfer resistance at the alloy/oxide interface shows a very minor dependence on the temperature, but a strong dependence on E_{pox} with a maximum at 0.2V, the same potential at which capacitance has a minimum. As the temperature increases to 70°C, the capacitance decreases.

Charge migration in the oxide shows a maximum value for E_{pox} in the range 0 - 0.2 V (depending on temperature). Oxide capacitance values show similar behavior and values at all temperatures for $E_{\text{pox}} < 0$ V. At more positive potentials at 70°C the film capacitance increases. By contrast at lower temperatures it decreases. This behavior suggests different film properties at 70°C compared to lower temperatures when $E_{\text{pox}} > 0$ V. This is supported by XPS data, which shows that at 70°C and $E_{\text{pox}} > 0.2$ V the concentration of non-stoichiometric Mo oxide increases while the Mo(VI) oxide decreased. At lower temperatures, the behavior is the opposite.

The need for a Warburg impedance to accurately fit the data indicates that defect diffusion occurs in the defective oxide. Values of L^2/D (where L is the effective diffusion thickness and D is the effective diffusion coefficient of the particle) calculated from the Warburg impedance show a minor dependence on E_{pox} at 30 and 50°C, but increase ~100 times at 70°C for E_{pox} in the range 0.4-0 V. Since ToF SIMS data show that the film thickness is increased at 70°C compared to lower temperatures, the decrease in L^2/D must be associated with an increase in mobility of electronic defects. This may be attributable to an increase in concentration of non-stoichiometric Mo oxide, a Mo(VI) oxide with a deficit of oxygen atoms, which would be expected to have high charge mobility.

For $E_{\text{pox}} < -0.4$ V and > 0.4 V a third component of the electrical equivalent circuit indicates a reaction impedance at the oxide/solution interface. The resistance for this surface reaction shows similar behavior at 50°C and 70°C, but the reaction capacitance values are different (at 50°C the capacitance increases over the potential range 0.4 V to 0.6 V, whereas at 70°C it decreases). This difference reinforces our argument that the oxide is different at 70°C. Experiments with alloys of different compositions would help elucidate these differences.

Oxygen Electro-Reduction on Passive Metals

Dominic Gervasio and Stephen P. Rogers
Arizona State University

Research Objectives

The objective is to examine the corrosion behavior of Ni-Cr-Mo alloys, using electrochemical and spectroscopic techniques, to estimate rate constants for oxygen reduction and passivation behavior on the alloys at different temperatures and alkaline water environments. This work is intended to provide inputs to models relating environmental factors to the corrosion processes of the alloys for the development of advanced analytical methods and next-generation conceptual models of the Ni-Cr-Mo alloys corrosion with significantly reduced uncertainty.

Approach

Cathodic redox reactions, such as oxygen (O_2) electro-reduction on the Ni-Cr-Mo alloys in alkaline water solutions, with and without salt additives (brines), are being studied to simulate the cathodic processes in thin layers of moisture and layers of moist particulates and deposits on metal surfaces. The O_2 reduction is of particular interest (although other redox reactions, such as nitrate reduction, may also contribute) as the source of cathodic current on the alloy surface that can sustain pitting, crevice corrosion, stress corrosion cracking, and galvanic action. A series of experiments were conducted to investigate O_2 reduction on fresh and/or aged alloy surfaces as a function of: electrical potential, temperature, and solution chemical composition. Results are important inputs to the determination of the onset and extent of cathodic stifling of corrosion processes. These experiments will provide input to modeling of corrosion of the Ni-Cr-Mo alloy, and the results provide a basis for model validation.

Two experimental apparatuses have been constructed and used for this project: (1) a rotating (gold) ring (Ni-alloy) disk electrode (RRDE) utilizing thermostatic control and a cycling potential ring method (CPRM) and (2) an electrochemical Fourier transform infrared (Echem-FTIR) cell using a photoelastic modulator for polarization modulated infrared reflection-absorption spectroscopic (PM-IRRAS) inspection of water layers near and surface monolayers on reflective Ni-Cr-Mo alloy surfaces. Results for the former are summarized here. The experimental apparatuses and techniques measure O_2 reduction, oxide growth, adsorbate-surface interactions, and other potential redox reac-

tions on passive metal as a function of potential and current. Research efforts have focused on:

- Measuring O_2 reduction on freshly polished Ni-Cr-Mo alloy surfaces in alkaline water solutions at different temperatures
- Characterizing the Ni-Cr-Mo alloy surface at different potentials and in different alkaline solutions
- Examining the effects of mechanical damage (scratch) to the passive film on Ni-Cr-Mo alloys.

Accomplishments

The voltammetry of Alloy 22 and Alloy C276 was performed in argon (Ar) de-aerated and O_2 saturated 1M KOH water solution at 30°C cycling between -0.6 V and 0.4 V versus saturated calomel electrode (SCE). The increasing capacitance of a Ni-Cr-Mo alloy electrode with each cycle suggests the accumulation of oxide on the alloy surface with each cycle. The voltammetry of the Alloy 22 and C276 is similar. These Ni-Cr-Mo alloys have similar compositions, with Alloy 22 having higher Cr (22% versus 16%) and lower Mo (13% versus 16%). Alloy C276 showed slightly lower capacitance (surface oxidation and reduction currents) at 30°C compared to Alloy 22 in Ar de-aerated alkaline water solution. That O_2 reduction was occurring on the alloy surfaces could be seen by the smaller semicircles in Nyquist plots obtained using Electrochemical Impedance Spectroscopy (EIS) of the alloys in O_2 saturated compared to Ar de-aerated alkaline water solution. Oxygen reduction is the most likely cathodic process for sustaining oxidative corrosion of a metal in air. Therefore, the rate of O_2 reduction current was quantified by the RRDE method as inputs to models of the rate of metal corrosion.

We were able to validate the CPRM RRDE methodology by repeating Vilambi and Taylor's work of O_2 reduction on a Au-ring and a Au-disk rotating electrode. The onset potential for O_2 reduction on Alloy 22 and Alloy C276, in alkaline water at pH 14, was approximately -0.6V, and it continued to -1.5V (vs. SCE). The CPRM study with a Ni-Cr-Mo alloy disk and Au ring showed strong evidence for O_2 reduction on nickel alloy surfaces by a series of two 2-electron steps. The rate constants, k_2 and k_3 , for these two steps were estimated, even though the limiting current for

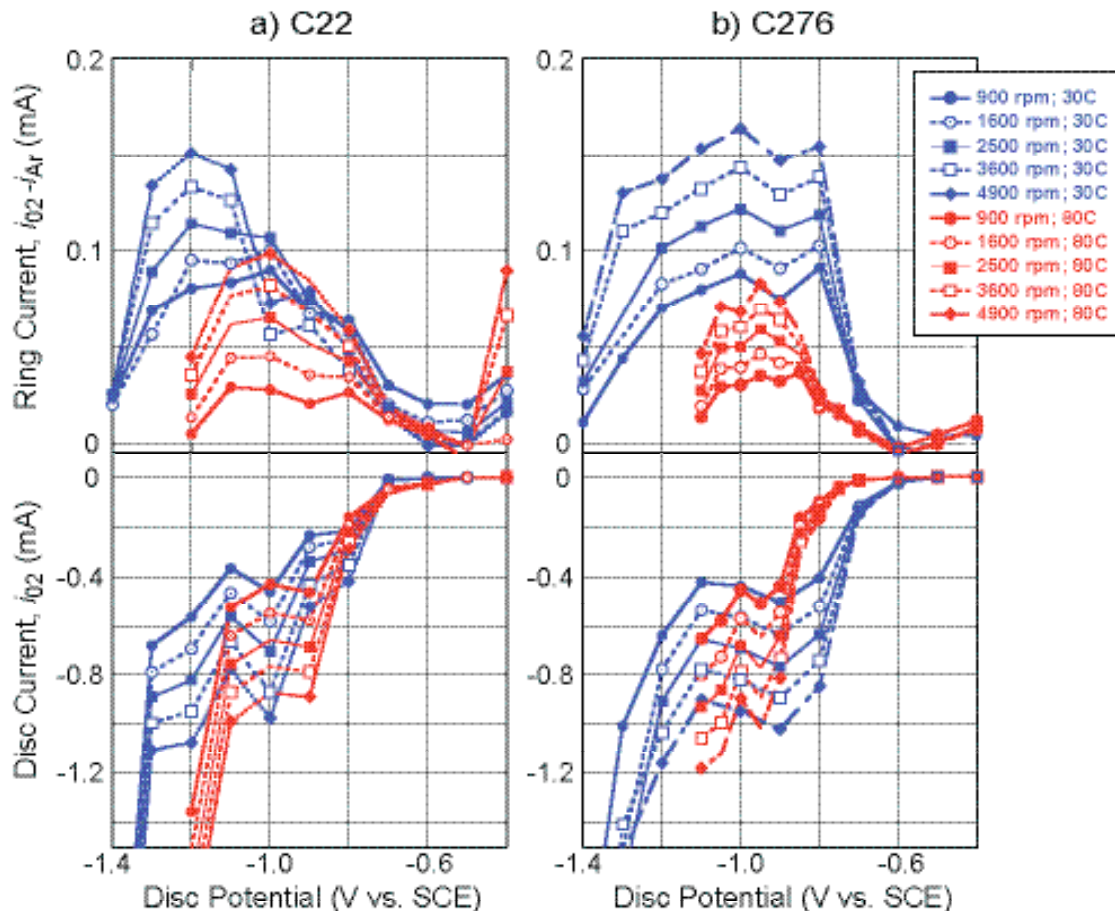


Figure 1. CPRM method (Au ring) to determine O_2 reduction on Ni-Cr-Mo alloy discs (a) Alloy 22 and (b) C276 in IM KOH (pH 14) at 30°C (in blue) and 80°C (in red).

the second step, peroxide reduction to water, was ill-defined because of its overlap with hydrogen generation due to the reduction of proton from water. At 30°C, the rate constants, k_2 (@ -0.7V for O_2 to H_2O_2) and k_3 (@ -1.2V for H_2O_2 to H_2O), were estimated to be 0.001 and 0.013 cm/s, respectively, for Alloy 22; and 0.193 and 0.232 cm/s, respectively, for Alloy C276. At 80°C, k_2 and k_3 were estimated to be 0.003 and 0.818 cm/s, respectively, for Alloy 22. The determinations of rate constants for O_2 reduction on nickel alloys at 80°C were more difficult owing to the poor seals of the Au ring and Ni-Cr-Mo alloy disc electrodes, and the enhanced H_2O reduction to H_2 at 80°C from the data in Figure 1.

In an additional task, infrared spectroscopy is being used to investigate the Ni-Cr-Mo alloy surface in an alkaline electrolyte under potential control. The alloy is behind an optical window housed in glass, PEEK, and Teflon. The cell is fixed to an optical bench with x-y, tilt, and rotation, and

both are in a nitrogen-filled box with feed-throughs to a potentiostat and cell-purge gases. This work is in a preliminary stage, and results will be reported in the next period.

References

- Vilambi, N. R. K. and E. J. Taylor, *Journal of Electroanalytical Chemistry*, 270, 61-77, 1989.
- Gervasio, D. and J. H. Payer, *Proceedings of the Electrochemical Society*, Orlando, FL, 58-70, 2003.
- Payer, J.H., B. Trautman, and D. Gervasio, *Methods Polymeric Materials Science and Engineering*, 68, 109-110, 1993.
- Pons, S, *Journal of Electroanalytical Chemistry*, 150, 495-504, 1983.
- Jiang, E, Y. and M. S. Bradley, A new approach to quantitative spectral conversion of PM-IRRAS: theory, experiments and performance comparisons with conventional IRRAS. ThermoFisher Scientific Application Note 01151.

Corrosion Cells Beneath Thin Films, Particulate, and Deposited Layers

Joe H. Payer, Pallavi Pharkya, Xi Shan, Arun S. Agarwal, and Hongyi Yuan
Case Western Reserve University

Research Objectives

The objective is to examine the behavior of macro- and micro-corrosion cells in experiments on passive metals covered by thin layers of moisture, particulate, and deposits. The operation of corrosion cells under these conditions can vary significantly from the behavior observed in fully immersed conditions. The corrosion of active metals, e.g., iron and zinc, in thin layers of moisture that pertain to atmospheric corrosion has been studied extensively; however, the behavior of passive metals in thin layers of moisture has received little attention. The results of this project will provide input to the modeling efforts to describe passive metal behavior. The foci are (a) the post-initiation stages of the corrosion cells to gain insight concerning the propagation, stifling, and arrest processes for localized corrosion; and (b) the durability of passive films beneath moist particulate and deposits.

Approach

A number of simulation cell configurations are used to investigate geometric effects, saturated and unsaturated particulate, chemical composition of moisture and particulate, temperature, and relative humidity. The current distribution and changes in chemical composition in thin layers of moisture and layers of moist particulate and deposits on metal surfaces are measured experimentally. The experiments are closely coupled to numerical modeling of corrosion cells. For passive film durability studies, the passive film properties are measured as a function of aging and the re-formation/repair behavior of the passive film after mechanical and/or chemical damage.

Accomplishments

Multiplate Cells for Simulation of Corrosion Cells

Of particular interest is the flow of current representative of corrosion scenarios to simulate the metal surface during pitting, crevice corrosion, stress corrosion cracking, and galvanic action. A range of layer thicknesses on metal surfaces is examined, i.e., from thin layers of absorbed moisture, to single particulate layers, to multi-particulate layers of 1 cm thickness and greater. A multiplate cell shown in Figure 1 was used to measure

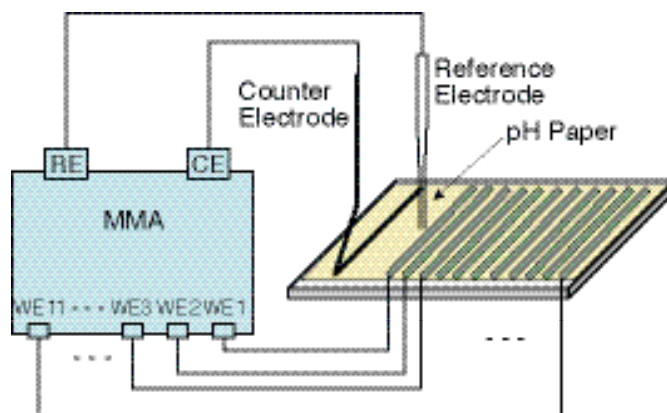


Figure 1. Schematic of multiplate cell to simulate crevice corrosion.

current distribution along the surface and chemical changes within the electrolyte for a simulated crevice-corrosion cell.

Cathodic current density was greatest on metal surfaces near the anode and fell off with distance away from the anode. As shown in Figure 2, the electrolyte became more alkaline on the cathode and more acidic on the

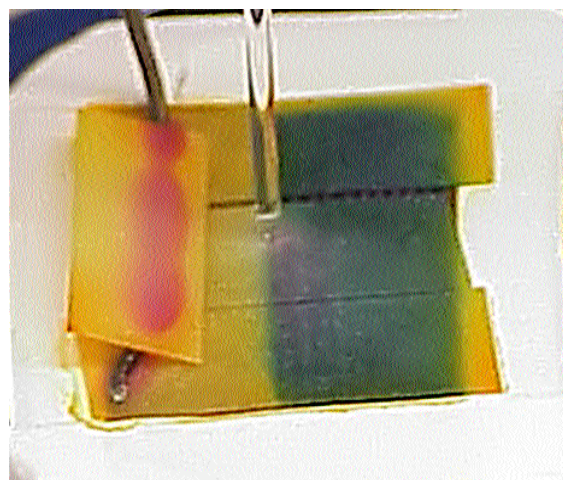


Figure 2. Chemical changes occur in the electrolyte layer due to hydroxyl generation on the cathodic surface (blue) and acid generation at the anodic surface (red).

anode. These chemical changes are more pronounced as electrolyte thickness decreases.

Durability of the Passive Film

The methods used are cyclic potentiodynamic polarization, constant potential scratch-repassivation, electrochemical impedance spectroscopy, and auger electron spectroscopy. The cyclic potentiodynamic polarization method determines corrosion properties such as corrosion potential, breakdown potential, repassivation potential, and passive range of the alloy. A scratch-repassivation apparatus, shown schematically in Figure 3, is used to examine the durability of the passive film after severe mechanical damage. The passive film that protects the metal is removed by scratching with a diamond-pointed scribe at rotation speeds to 100 rpm. The amount of damage and repassivation behavior is examined by monitoring the anodic current from the specimen and by post-test surface examination. For controlled potentials within the passive range, the corrosion current from Alloy 22 decreased rapidly after the metal was scratched, indicating rapid repassivation (Figures 4 and 5). Preliminary surface analysis and electrochemical impedance spectroscopy found no significant change in the passive film properties before and after mechanical damage.

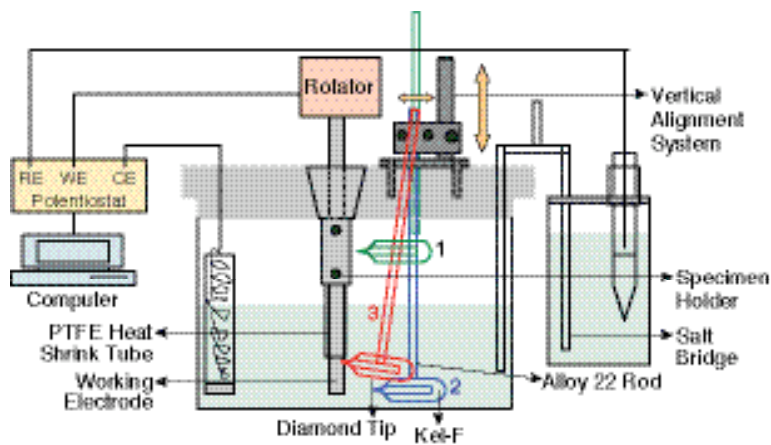


Figure 3. Schematic of scratch-repassivation apparatus with controlled rotation speed.

This project examines corrosion and passive film durability in thin moisture films and layers of particulate and deposits. Results are important inputs to determine the durability of the passive films that are responsible for the high corrosion resistance of Ni-Cr-Mo alloys and to determine the evolution of corrosion damage over long periods of time. The findings are beneficial to development of advanced, next-generation models and alternative conceptual models. A better scientific understanding of the chemical, electrochemical, and corrosion processes is provided.

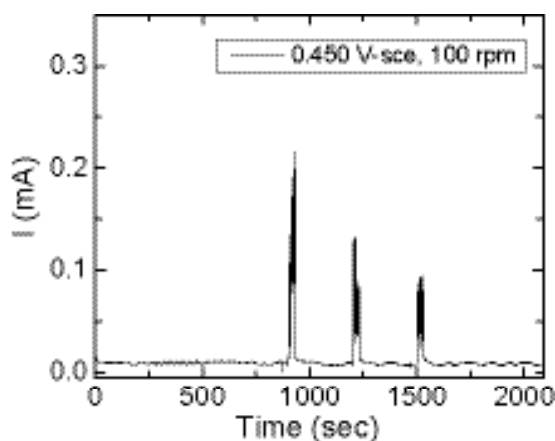


Figure 4. Scratch-repassivation behavior of Alloy 22 after scribing with a diamond tip at 15th, 20th, and 25th minute at $+0.450 V_{SCE}$ in 0.6M NaCl (open to air), $80^{\circ}C$ at rotation speed of 100 rpm. The passive film reformed after each scribing event.

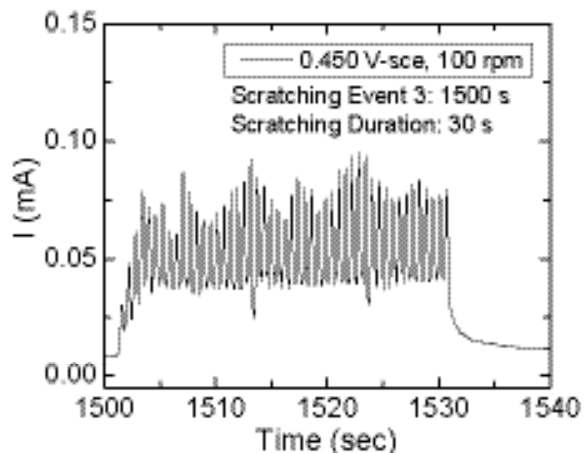


Figure 5. Current-time transients of Alloy 22 at 25th minute under the same experimental condition as in Figure 4.

Electrochemical Measurements of Corrosion under Thin Brine Layers

Gerald S. Frankel, Rudolph G. Buchheit, Bastian Meier, and Shoichiro Taira
Ohio State University

Research Objectives

The objective is to make electrochemical measurements on corrosion-resistant alloys under thin electrolyte layers representative of dust, particulate, and adsorbed moisture (from monolayers to millimeters in thickness); and characterize the relationship between the physical characteristics of the layers and the electrochemical behavior of the alloys.

Approach

A major challenge in making electrochemical measurements in thin electrolyte layers is the incorporation of a viable reference electrode with the ability to provide spatial resolution of the potential. In this task, Kelvin Probe (KP) and Scanning Kelvin Probe (SKP) techniques are utilized to make electrochemical measurements in the thin layers. The KP provides a noncontact measurement of potential. Since the KP is limited to room temperature operation, high-temperature measurements are made with an in-plane Ag/AgCl electrode. This approach is being used on Alloys 276 and 22 at temperatures up to 120°C. A schematic drawing of the glass chamber used is shown in Figure 1. The RH was controlled by the saturated salt solution in the bottom of the chamber. The whole chamber was placed in a furnace to fix the temperature. The open circuit potential (OCP) is monitored; a sudden drop in OCP is an indication of localized corrosion initiation.

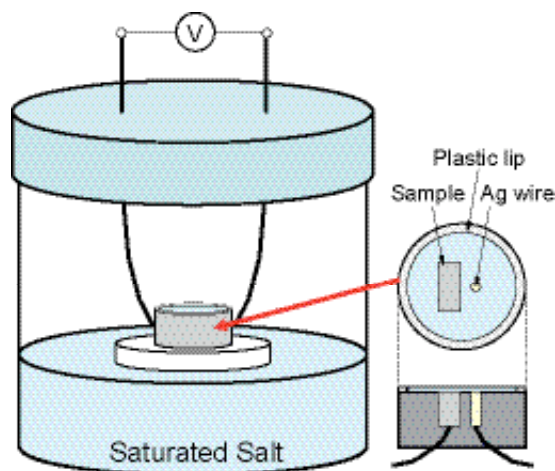


Figure 1. Schematic diagram of the cell for corrosion potential measurement.

In another approach, mineral deposition on Alloy 22 was simulated by cathodic reactions. The scenario being explored is precipitation of Ca^{2+} ions from thin layer solutions that become alkaline due to oxygen reduction occurring on the alloy surface. Mineral deposition was induced by cathodically polarizing Alloy 22 electrodes in saturated boiling CaCO_3 or $\text{Ca}(\text{NO}_3)_2$ at a potential of $-0.2V_{\text{sce}}$ for two hours. To determine if the resulting deposits retarded or aggravated corrosion during subsequent exposure to a hot chloride solution, the modified electrodes were potentiodynamically polarized in a 5M NaCl solution or a 4M NaCl + 2M KNO_3 solution.

Accomplishments

OCP Measurements with a Kelvin Probe during Electrolyte Drying

Drying experiments were performed with layers of chloride solutions on SS304 to investigate the influence of the initial electrolyte volume or the final electrolyte thickness on the pitting initiation time. As an electrolyte dries, the concentration increases. A volume of 0.5 M MgCl_2 solution was spread over the SS304 sample, and then air with low (33%) humidity was flowed through the KP chamber. This results in a slow drying of the MgCl_2 solution and an increase in the Cl^- concentration until pitting occurs. No dependence of the pitting initiation time on the electrolyte volume or the final electrolyte thickness was found.

Similar experiments were carried out with silica-covered SS304 to simulate rock dust on the surface. The silica layer was applied by cathodic electrophoretic deposition, and varying deposition time was used to simulate different dust layer thickness. A volume of 0.5 M MgCl_2 again was spread over the coated SS304 sample, which was put in the KP chamber with a constant relative humidity of around 33%. The initiation of pitting as indicated by a drop in OCP was monitored. Silica layer thickness had no effect on pitting initiation time.

To determine the critical chloride concentration for pitting corrosion on 304 stainless steel, the corrosion potential and the solution layer thickness were monitored simultaneously with the Kelvin Probe. A volume of 0.44 M MgCl_2 solu-

tion was put on the SS304 surface, and the chamber was purged continuously with air of constant 33% relative humidity. The critical chloride concentration was calculated from the electrolyte thickness at the point of pitting initiation and the exposed area. This concentration was found to lie between 5.1 M and 9.8 M.

Measurements at High Temperature

The cell shown in Figure 1 was used in this work. The alloy sample was mounted with an Ag wire in epoxy resin, and polished with SiC paper up through 1200 grit. The Ag wire was chloridized prior to the experiment. A volume of 1M LiCl was spread on the surface, and saturated LiCl solution was placed at the bottom to keep the relative humidity constant. The glass container was then placed in a furnace and the potential between the sample and the Ag/AgCl electrode was monitored. With time, the LiCl solution layer thinned and approached saturation, which is known to be about 30 M in hot water. Figure 2 shows the change of OCP with time for Alloys 276 and 22 at 90°C and 120°C. In the case of Alloy 22, the OCP became constant after a few hours for both temperatures; the value for 120°C was higher than that for 90°C. For Alloy 276, the OCP was similar to that of Alloy 22 at 90°C. However, at 120°C the OCP decreased steadily for the first 5 hours and then precipitously dropped by about 200 mV.

The samples were analyzed with an optical microscope after the experiment, and pits were observed only for Alloy 276 at 120°C. Figure 3 shows an optical microscopy image and atomic force microscopy (AFM) characterization of the pits, which were found to have a diameter of about 6 μm and depth of 300 to 500 nm. These results show that Alloy 22 is resistant to pitting at OCP even in 30M Cl⁻ at 120°C, whereas Alloy 276 is not.

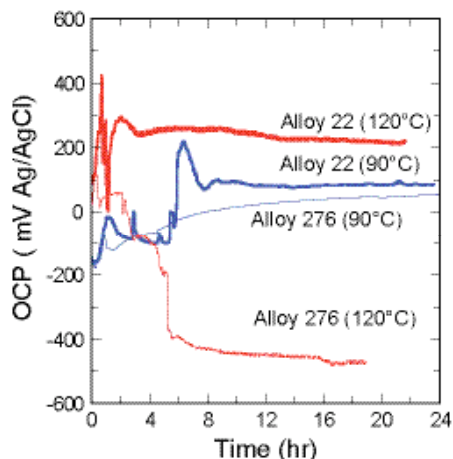


Figure 2. Variation of open circuit potential with time for Alloys 22 and 276 at 90°C and 120°C.

Mineral Deposits

Results of this study show that cathodic polarization can contribute to the deposition of an adherent mineral layer from Ca²⁺-bearing solutions. The effects of this layer on subsequent corrosion behavior in chloride and chloride-nitrate solutions are mixed. In general, Ca mineral layers formed in these experiments partially block the surface. After mineral deposition, the passive current density is reduced by one to two

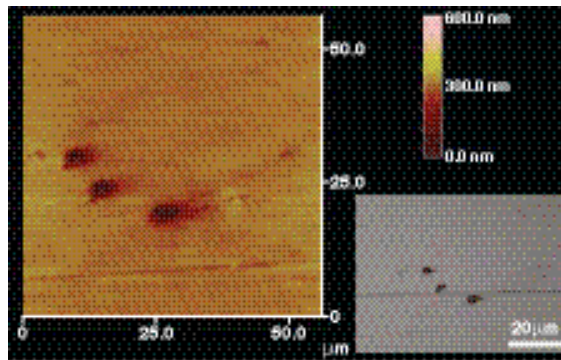


Figure 3. Morphology of pits formed on Alloy 276 at 120°C characterized by AFM and optical microscope picture of same area.

orders of magnitude. Part of this reduction is due to blocking of the surface by the mineral layer, but as suggested by increases of up to 200 mV in the corrosion potential, there may be a decrease in the true passive current density that contributes to the observed reduction. In both chloride and mixed chloride-nitrate environments, the presence of the mineral layer appears to lower the pitting potential for the onset of transpassive dissolution. Repassivation potentials are also lowered in the majority of cases. In post-test scanning electron micrographs there is clear evidence that localized corrosion occurs under and at the periphery of these deposits (Figure 4).

Figure 4. Localized corrosion under Ca mineral deposits after cyclic polarization in a mixed chloride-nitrate solution.

Mechanism of Mixed-Ion Effects on Corrosion in Thin Films

Roger C. Newman and Christopher Healey
University of Toronto

Research Objectives

This project is designed to extend the artificial pit technique to thin particulate layers, applying similar rigorous mass transport analysis to that used in bulk solutions. We are applying the extended technique to investigate mixed ion effects on corrosion in thin films. A major focus is on nitrate inhibition of localized corrosion in chloride solutions.

Approach

The artificial pit, or pencil electrode, technique involves embedding a metal wire in resin and dissolving it from one end in a salt solution, so that the entire exposed surface acquires the condition of a localized corrosion surface (pit or crevice). This creates a one-dimensional mass transport condition while simulating the metal dissolution and solution alteration (pH, [Cl⁻]) that occur within natural localized corrosion sites. The simplified mass-transport condition enables us to determine unambiguous kinetic parameters and to study the effect of inhibiting substances such as nitrate ions. It is important to note that with modern instrumentation, the currents that can be measured from such electrodes cover the whole range from penetration rates of microns per second, to those that are of concern for the long-term propagation of tight crevices or underdeposit events in equipment, e.g., microns per year.

The conditions chosen for the study were dilute chloride and chloride/nitrate solutions, at a temperature range of 75–95°C. A series of Ni-22Cr-xMo alloys were fabricated into thin wires and used as artificial pit electrodes.

We have shown, for the first time, that it is relatively straightforward to grow one-dimensional artificial corrosion cavities in thin, moist particulate layers—by mounting the electrode in resin within concentric Ag and Pt rings acting as reference and counter electrodes, respectively. A moist particulate layer is applied, and initiation and propagation of corrosion are easily monitored. Differences have been detected between thin layer and bulk-solution behavior. These are not always

in the direction expected. Impedance measurements between concentric chloridized Ag ring electrodes are used to monitor the properties of the moist layer and to examine reproducibility.

Accomplishments

In this period, we made major improvements in the humidity chamber used to expose the corrosion sensors with thin particulate layers while making electrochemical measurements. Two samples can now be exposed under different conditions, and a drawer arrangement has been added to facilitate rapid changes of the salt solution that controls the humidity. An improved humidity sensor rated to 100°C has been installed.

We have compared kinetics in bulk and thin-film conditions for pure chloride solutions, assuming in the first instance that equilibrium prevails so that the aqueous phase within the particulate layer is the same as that in the bottom of the chamber. It is recognized that there may be detailed differences, due (for example) to capillary effects or the impact of hygroscopic corrosion products. Most experiments have been done in near-saturated NaCl conditions. Then, we developed methods to inoculate nitrate into the particulate layer while the pit was growing under electrochemical control. Initially this was done by spraying, but now a spotting technique is used. This aspect is under further development.

Figure 1 shows a typical repassivation transient for a relatively resistant alloy upon inoculation of nitrate to a relatively high level. In all such experiments performed to date, ingress of the newly added ion into the pit was more rapid than expected, and even more rapid than in a bulk solution. This highlights that we still have much to learn about the details of mass transport in such systems where capillary effects coexist with diffusion.

A peculiar phenomenon was observed when monitoring the impedance between concentric silver electrodes in thin particulate layers. Despite a fairly low solution resistance between the silver electrodes, the

corrosion process would not stabilize, possibly because the pit solution itself dries out the nearby particulate layer.

Next steps will involve the greater occlusion of the cor-

rosion cavity, to simulate in a short time the low limiting anodic current density under a dense membranous deposit that might take many years to form in practice, followed by further evaluation of the effect of nitrate inoculation.

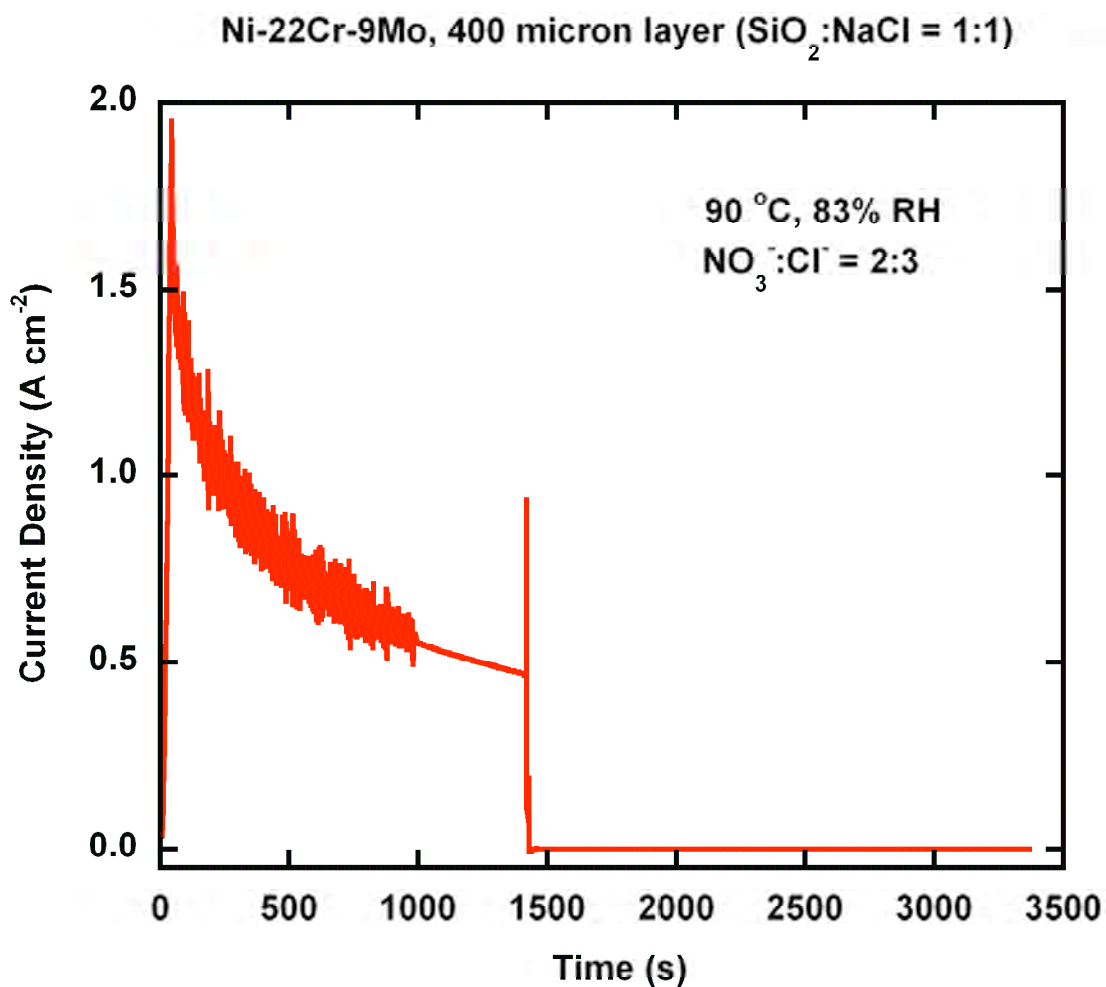


Figure 1. Repassivation of a corrosion cavity in a thin particulate layer due to the inoculation of nitrate (reduction in the noise after 900 s is due to dropping the potential from 900 mV to 325 mV (Ag/AgCl)). Nitrate inoculation at 1420 s.

Effect of Environmental Variables on the Structure and Composition of Passive Films

Tzipi Cohen-Hyams, Marcela Miyagusuku, Scott Harrington, and Thomas M. Devine
University of California, Berkeley

Research Objectives

The focus of our research is the identification of the passive films that are responsible for the corrosion resistance of Alloy 22 and the determination of the film's fundamental properties that affect its protective nature.

Approach

When passive films are removed from aqueous solutions, structure and properties can change. To avoid this, the present study uses five *in situ* techniques to examine passive films in a series of aqueous electrolytes: (1) chloride-free and chloride-containing solutions of near-neutral pH, typical of many engineering applications of passive alloys; (2) acidic solutions (0.001M–12M HCl) that mimic the electrolytes inside pits and crevices and that can severely damage the passive metals; and (3) neutral and acidic solutions with nitrate and sulfate ions, which may inhibit localized corrosion by chloride.

Identical experiments are conducted on Alloy 22 and its major alloying elements: Cr, Ni, Mo, and Fe. Results of tests conducted on the metallic elements help to interpret the results of tests performed on Alloy 22. Tests are also conducted on several alloys that, like Alloy 22, are protected by chromium-rich passive films: Alloy 600 (Ni-Cr-Fe) and 304 stainless steel (Fe-Cr-Ni). Comparing and contrasting the results of tests conducted on Alloy 22, Alloy 600 and 304 SS indicate the influence of alloy composition on the structure, composition, and properties of Cr-rich passive films.

Accomplishments

Although the corrosion resistance of the alloys investigated is largely determined by the alloy's chromium concentration and the passive films of each alloy are mainly Cr-rich oxides/hydroxides/oxyhydroxides, our results have revealed that the chromium-rich films formed on Alloy 22, Alloy 600, 304 SS, and pure chromium are all different. The *in situ* Surface Enhanced Raman (SER) spectra of the passive films formed on chromium and Alloy 22 at -0.2V vs. Ag/AgCl in 1M HCl are presented in Figure 1 and illustrate the point. The spectra are clearly different. The combination of peaks present in the SER spectra of chromium's

passive film approximately match the set of peaks associated with CrIII-O bonds, but do not match the spectra of known oxides and hydroxides of chromium. Accordingly, chromium's passive film in 1M HCl is best characterized as an amorphous CrIII oxide.

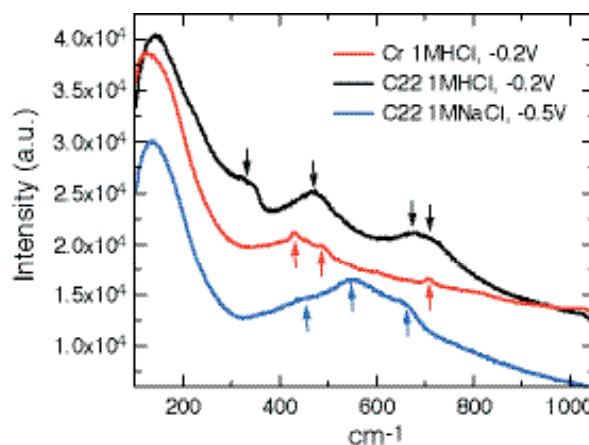


Figure 1. SERS of passive films of Cr and Alloy 22.

The peaks present in the SER spectrum of the passive film formed on Alloy 22 have not yet been assigned. Suffice to say, the spectrum does not match the spectrum of any known oxide/hydroxide of chromium. It is possible that molybdenum is present in the Alloy 22 passive film, but it is unlikely that nickel or iron contribute significantly to the Alloy 22 passive film in 1M HCl, since films were not formed on unalloyed nickel or iron in 1M HCl. At this time, it is safe to say that the passive films of Alloy 22 and Cr in 1M HCl are quite different.

In addition to the alloy's composition, the passive film depends on the pH of the electrolyte. Comparison of the SER spectra of Alloy 22 in 1M NaCl (-0.5V) and in 1M HCl (-0.2V) illustrates the strong influence of the electrolyte pH on the identities of Alloy 22 passive films (0.5V in 1M NaCl and -0.2V in 1M HCl have approximately the same hydrogen overpotential). The three, broad, overlapping peaks in the SERS of Alloy 22 film in 1M NaCl are tentatively assigned to a mixture of Ni(OH)₂, which is most likely an outer layer, and NiCr₂O₄. Thus, lowering the pH from approximately 5.5 (1M NaCl) to 0 (1M HCl) converts the passive film from a mixture of Ni(OH)₂ and NiCr₂O₄ to an amorphous Cr(III) oxide.

Our SERS results indicate that anions present in the electrolyte can absorb into the outer layer of the passive films. In chloride-free borate buffer (pH8.4) there is a critical potential above which borate ions absorb into the passive films. The ions are thought to absorb into the outer layer of the film rather than adsorb on the film's surface, because the anions remain part of the SER spectra until the potential is lowered considerably below the critical potential. A similar result was obtained for chloride ions in tests conducted in 1M NaCl and 1M HCl.

Electrochemical Quartz Crystal Microbalance (EQCM) measurements, Cyclic Polarization (CyP), Electrochemical Impedance Spectroscopy (EIS) and Mott-Schottky analysis (M-S) provide valuable information about various properties that strongly influence the protectiveness of the passive films. For example, EQCM measurements of chromium in borate buffer indicate that the formation of the passive film is not 100% efficient. That is, only a portion of the overall oxidation current goes into film growth. The remainder is attributed to alloy dissolution. Given that SERS indicates each of the Cr-rich passive films formed on Alloy 22, Alloy 600, Alloy 304SS, and unalloyed Cr, are different, it will be instructive to use EQCM to determine how protective each passive film is by measuring how much alloy dissolution accompanies film growth.

The combination of CyP, SERS, and EQCM tests have been especially valuable in investigating the oxidation of Cr0 to CrVI, a reaction that occurs at relatively high potentials and is thought to have an important negative influence on the alloy's resistance to pitting corrosion. Our results have found that Cr0 is oxidized to CrVI by a two-step process consisting of Cr0 \rightarrow CrIII, followed by CrIII \rightarrow CrVI. At least some (if not all) of the CrVI is formed within the CrIII film, rather than at the film/electrolyte interface. The rate of the electrochemical reduction of CrVI formed during anodic polarization was unaffected by stirring of the electrolyte.

The EIS measurements indicate the films have very narrow space charge regions, <1 nm, which is consistent with the high values of immobile charge density ($\sim 10^{+21}$ /cc) measured by M-S plots. The M-S plots also indicate the values of the flat band potentials of the passive films. The flat band potentials measured for Cr and Alloy 22 passive films in 1M HCl, 0.1M HCl, 0.1M H₂SO₄ + 1M NaCl, 1M NaCl, and 0.1M borate buffer (pH8.4) are presented in Figure 2, along with the calculated values of the hydrogen equilibrium potential. In all electrolytes tested, the flat band potentials of Alloy 22, V_{fb} (Alloy 22), are approximately equal to the

hydrogen equilibrium potential, $\Delta\phi_e(H)$, which indicates equilibrium between electrons in Alloy 22 passive film and electrons in the H/H⁺ redox couple. An alternative interpretation is that Alloy 22 passive film is so thin that electrons in Alloy 22 are in equilibrium with electrons in the H/H⁺ redox couple – i.e., electrons can tunnel through the film from (to) states in the alloy to (from) states in the H/H⁺ redox couple.

The low value of $V_{fb}(Cr)$ relative to the hydrogen equilibrium potential suggests that the flat band potential of Cr passive film is determined by ion adsorption rather than by electron transfer, which, as discussed above, is the case for the Alloy 22 passive film. That is, the flat band potential of Cr passive film is that potential at which the rates of ion

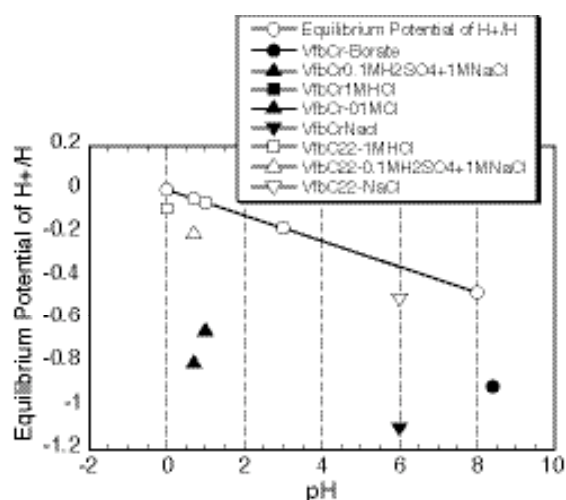


Figure 2. $V_{fb}(\text{Alloy 22})$ – open points, and $V_{fb}(\text{Cr})$ – solid points as a function of electrolyte's pH.

adsorption and desorption are equal. The largely different values of $V_{fb}(\text{Alloy 22})$ and $V_{fb}(\text{Cr})$ are consistent with the different SER spectra of Alloy 22's and Cr's passive films. The low value of $V_{fb}(\text{Cr})$ compared to the value of $V_{fb}(\text{Alloy 22})$ is also consistent with the higher rate of H⁺ reduction on the surface of Alloy 22 than on the surface of Cr.

In summary, our comprehensive *in situ* investigation of the passive films of Alloy 22, using five different experimental techniques, indicate the films are chromium-rich, but are distinct from the chromium-rich passive films that form on unalloyed chromium and on other nickel-chromium and iron-chromium alloys. The identities of the films are strong functions of the electrolyte's pH and the potential of film-formation.

EVOLUTION OF CORROSION DAMAGE BY LOCALIZED CORROSION

Crevice-Corrosion Electrochemistry of Ni-Cr-Mo Alloys

John R. Scully, Florent Bocher, and Francisco Presuel-Moreno, University of Virginia

Modeling of Critical Chemistry for Crevice Corrosion

Robert G. Kelly, Andrew J. Hodges, and Francisco Presuel-Moreno,
University of Virginia

Crevice-Corrosion Damage Function on Alloy 22

David W. Shoesmith, Dmitrij Zagidulin, P. Jakupi, and James J. Noël,
University of Western Ontario

Localized Corrosion Stability in the Presence of Non-Chloride Anions

Roger C. Newman and David X. He, University of Toronto

Metallurgical Effects on Localized Corrosion of Ni-Cr-Mo Alloys

Gerald S. Frankel, Rudolph G. Buchheit, Ajit Mishra, and Federico Gambina,
Ohio State University

Processes in Crevice-Corrosion Propagation, Stifling, and Arrest

Joe H. Payer, Xi Shan, Arun S. Agarwal, and Uziel Landau,
Case Western Reserve University

Combinatorial Chemistry Approaches for Alloy Composition and Corrosion Behavior

Rudolph G. Buchheit, Gerald S. Frankel and Fariaty Wang, Ohio State University

Prediction of the Time Evolution of Localized Corrosion Damage

Digby D. Macdonald, Igor Nistic and George R. Engelhardt, Pennsylvania State University

This page intentionally left blank.

Crevice-Corrosion Electrochemistry of Ni-Cr-Mo Alloys

John R. Scully, Florent Bocher, and Francisco Presuel-Moreno
University of Virginia

Research Objectives

The objective of this project is to understand the impact of electrochemical driving force (e.g., applied potential), physical and geometric conditions (e.g., temperature and crevice gap/depth), and unconventional crevice-former properties (e.g., semi-permeability and reactivity) on the crevice-corrosion susceptibility of Ni-Cr-Mo alloys. The test conditions and materials were selected to provide insight into the crevice corrosion of Alloy 22 (UNS N06022) in high-temperature multispecies brines. Additionally, crevice formers will simulate dust, debris, and other deposits. Lesser corrosion-resistant materials such as stainless steel AISI 316 (UNS S31600), Alloy 625 (UNS N06625), and a family of Ni-Cr-Mo alloys were introduced for comparison to Alloy 22.

Approach

The focus is on the combination of anodic material properties, and physical and electrochemical conditions, that govern crevice corrosion of Ni-Cr-Mo alloys. Consequently, various test conditions are being implemented, including: proximate cathodes, limited and infinite cathodes, and porous crevice formers. Proximate and limited cathodes are linked to crevice corrosion occurring within a limited volume of solution (e.g., droplets such as might exist on a metal surface) where the cathode will be next to the crevice mouth and its current capacity will be limited by the wetted area outside the crevice. The porous crevice-former experiments are associated with the characteristics of the real life crevice formers, e.g., pieces of rock and dust particles. Some of these unconventional crevice-former characteristics have been reproduced in a controlled fashion, for instance by using O₂-permeable crevice-former materials. The crevice-corrosion behavior of stainless steel AISI 316 and Alloys 625 and 22 under these conditions is being compared. This is accomplished by studying crevice corrosion initiation, propagation, and repassivation and/or stifling using coupled multi-electrode arrays in rescaled crevices, as well as with conventional multi-crevice assemblies (MCA), to verify trends seen in rescaled crevices. Scaling laws are used to rescale the crevice geometry to a larger length scale while keeping the electrochemical corrosion properties similar to those of a smaller natu-

ral crevice. Coupled multi-electrode arrays (CMEA) consisting of close-packed coupled electrodes are capable of obtaining local electrochemical information as a function of spatial location within crevices. CMEAs can provide combined spatial and temporal resolution of electrochemical properties within the rescaled crevice. The rescaled crevice provides unprecedented information on how a crevice anode initiates, propagates, and reorganizes under realistic conditions.

A related objective is to characterize Ni-Cr-Mo alloys' corrosion electrochemistry focusing on active dissolution properties relevant to isolated anodes, as a function of well-controlled artificial, acid-chloride crevice solutions. The solution chemistries for crevice corrosion range from solutions saturated in metal salts to dilute bulk solutions. The effects of metal alloy composition on conditions for depassivation and activation as well as active corrosion rates are determined. Critical crevice chemistries for active dissolution are defined. The anodic polarization behaviors of model Ni-22Cr-XMo alloys, Alloy 22 and Alloy 625, were previously studied in hydrochloric acid of various concentrations to crudely simulate critical crevice solutions at various percentages of dilution. In order to more accurately simulate crevice solution and crevice anode electrochemistry, HCl has been replaced by LiCl+HCl solution in this project to enable the independent control of the total chloride content and the pH and to provide more realistic simulants of crevice anolytes. The anodic polarization behaviors of alloys 625 and 22 as well as Ni-22Cr-XMo model alloys (X = 0, 3, 6, 9 and 13) are under study, using single microelectrodes in LiCl + HCl solutions. This E-i polarization behavior complements crevice studies and is used to help understand crevice behavior in CMEA. Subsequent modeling studies examine whether these electrochemical conditions can be met in realistic crevices. Data from isolated anode microelectrodes are free of artifacts and geometric effects, and thus can serve as valid E-i boundary conditions for input to modeling studies.

Accomplishments

A database of E-i polarization behavior of model Ni-22Cr-XMo (X=0, 3, 6, 9 and 13) in HCl solutions of different concentrations (0.1 M, 1 M and 10 M HCl) and at different

temperatures (22°C, 50°C, and 85°C) was established and extended to alloys 625 and 22. Anodic polarization of those two alloys was also investigated in LiCl + HCl based solutions. These solutions' compositions are derived from the alloys' Ni, Cr, Mo, and Fe content, assuming congruent dissolution of the alloys and hydrolysis of Cr³⁺ as the main source of hydronium ions. The effect of the chloride concentration on the hydronium's activity is also taken into account.

The anodic polarization data provide E-i boundary conditions that are used to derive scaling laws. Scaling laws provide information concerning the crevice G/x_{crit}^2 ratio (G : crevice gap, x_{crit} : critical crevice length where crevice corrosion initiates). The relationship between G and x_{crit}^2 is linear up to a crevice gap of approximately 30 microns, depending on the materials, conditions, and model crevice-corrosion solutions used. For a given gap and equivalent environment, i.e., temperature and model crevice solution, it is found that the distance x_{crit} increases with the pitting resistance equivalent number (PREN) of the Ni-Cr-Mo alloys.

The array design provides the flexibility of arranging a number of electrodes both inside and outside of the crevice, so that the effect of highly aggressive crevice solution leaking outside the crevice can be studied. In a bulk environment of 0.6M NaCl, crevice corrosion initiates at higher potentials and temperatures as the PREN of the material increases. The initiation and propagation of crevice corrosion on a CMEA for Stainless Steel 316 and for Alloy 625 are shown in Figure 1 (a) and (b), respectively. It is notable that no crevice corrosion was observed for Alloy 22 at 50°C. Alloy 22 only suffered crevice corrosion at 90°C. This is consistent with the fact that its critical crevice temperature is reported to be approximately 85°C.

The impact of a proximate cathode on crevice corrosion of AISI 316, and Alloys 22 and 625 was also determined. It was found that, in the presence of a proximate cathode, crevice-corrosion initiation required a much higher applied potential and only occurred at deeper depths from the crevice mouth. The value of x_{crit} may increase beyond the physical depth of the debris when the cathode is close.

Crevice corrosion of a multi-crevice assembly (MCA) was initiated at high potentials using an infinite cathode

(potentiostat) and switched to galvanic coupling with decreasing finite cathode area. The effect of limited cathodic current on propagation and stifling of crevice corrosion is also studied for Alloys 22 and 625. These studies will be repeated using CMEAs.

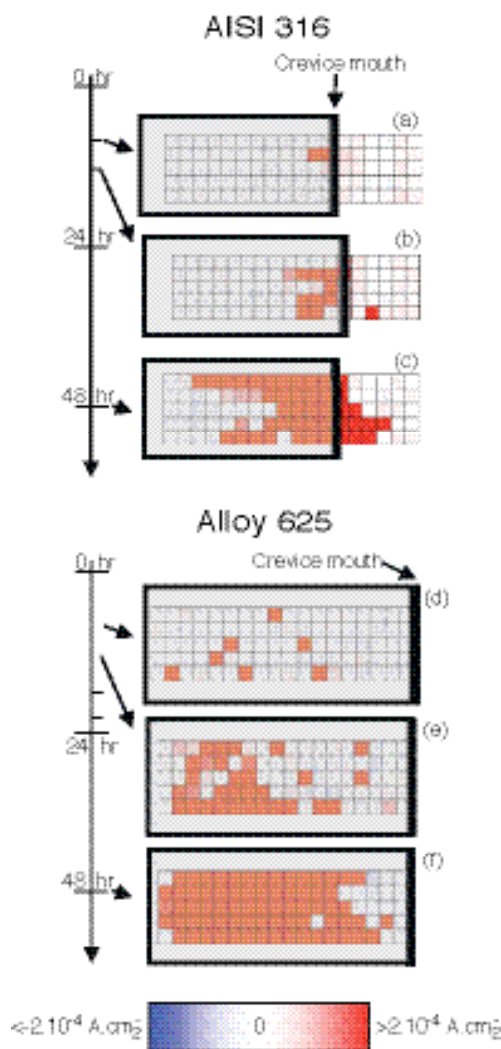


Figure 1. Comparison of crevice-corrosion initiation and propagation between stainless steel AISI 316 and Alloy 625 in 0.6 M NaCl at 50°C. The crevice mouth is indicated by the bold black line and the covered area within the shaded rectangle (not up to scale with the real life crevice former). (a) 7 hrs at 0 V_{SCE}, (b) 11 hrs at 0 V_{SCE}, and (c) 24 hrs at 0 V_{SCE} + 24 hrs at 25 mV_{SCE}; (d) 18 hrs at 50 mV_{SCE}, (e) 22 hrs at 50 mV_{SCE}, and (f) 24 hrs at 50 mV_{SCE} + 24 hrs at 75 mV_{SCE}. "SCE" is saturated calomel electrode.

Modeling of Critical Chemistry for Crevice Corrosion

R.G. Kelly, Andrew J. Hodges and Francisco Presuel-Moreno
University of Virginia

Research Objectives

A primary goal of this work is to establish a stronger scientific basis for the calculation of the stability of crevice-corrosion propagation for corrosion-resistant alloys (i.e., stainless steels, Ni-Cr-Mo-Fe alloys) under atmospheric exposure conditions. Of particular interest is the current demanded by a localized corrosion site as a function of crevice geometry, temperature, alloy composition, RH, and external solution layer composition. Augmenting this work has been the experimental study of crevice-corrosion stability using crevices with rigorously defined geometries.

Approach

A previously developed crevice-corrosion computational code has been used to probe the ability of a crevice to maintain a region of active corrosion. The crevice has a set gap and length. The electrochemical kinetics for the Type 316L stainless steel and Ni-22Cr-6Mo were abstracted from literature data or from other projects in the DOE Corrosion Cooperative in order to quantify the effects of pH and chloride concentration on the dissolution kinetics. A series of crevice gap/length combinations were studied in which the initial solution within the occluded region was set to be sufficiently aggressive as to activate crevice corrosion. A transient analysis of the mass transport allowed a determination of whether that crevice corrosion could remain active – whether the dissolution within the crevice was sufficient to create additional low pH, high chloride solution faster than it could diffuse out of the crevice. In addition, the effects of high chloride concentrations on the activity of the hydrogen ion (leading to lower effective pH values) and on the conductivity were considered, as were the effects of the presence of cathodic reactions within the crevice.

The experimental work used microfabrication methods to produce crevice samples with gaps between 3 and 11 microns, and lengths between 1 and 8 mm. Experiments were conducted on Type 316 stainless steel in which the crevice was filled with an aggressive solution (pH < 1.5, [Cl⁻] > 1 M) before immersion in an electrolyte and the application of an applied potential. The ability of the crevice to maintain active corrosion was monitored by

measurement of the current. The initial solution composition was sufficiently aggressive to depassivate the surface. If the crevice geometry was not sufficiently occluded to maintain the critical chemistry, the crevice repassivated. Conversely, if the geometry restricts mass transport out of the crevice sufficiently, the dissolution rate can maintain the critical chemistry despite diffusion out of the crevice. Afterwards, crevice attack was verified and its location and depth quantified with a confocal laser scanning microscope.

Accomplishments

The results of the modeling work show that the effects of the high chloride ion concentration on the activity coefficient for the hydrogen ion and conductivity are important in crevice stabilization. Figure 1 shows an example for Type 316L stainless steel. For a 1.2 micron gap, crevice corrosion is predicted to be stabilized only if these effects are taken into account. If they are not considered in the model, the crevice repassivates, i.e., the current rapidly falls to low values and decreases with longer times. It was also found that inclusion of cathodic reactions within the

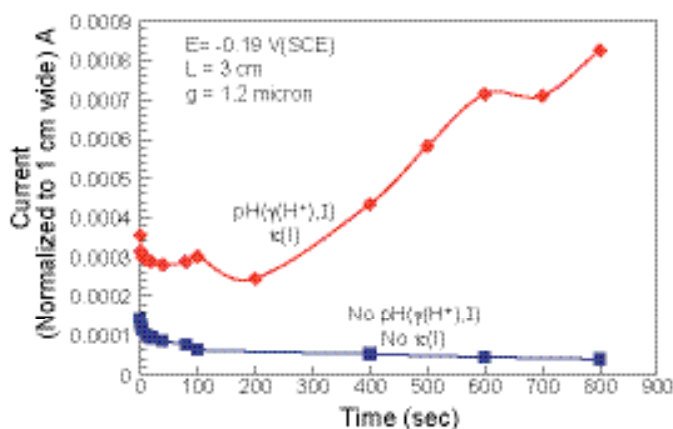


Figure 1. The effect of high chloride concentration (in terms of ionic strength, I) on the stabilization of crevice corrosion in Type 316L stainless steel.

crevice hindered stabilization. The hindering of stabilization is due to the creation of hydroxyl ions within the crevice. These ions act to neutralize the acidity that is produced by the hydrolysis of the chromium formed by dissolution. As crevice corrosion can only be stabilized if the

crevice solution becomes highly acidic, the formation of hydroxyl within the crevice makes attainment and maintenance of the critical chemistry more difficult, and thus a tighter gap or more rapid dissolution kinetics are required.

Work on the Ni-22Cr-6Mo alloy showed that an initial crevice solution pH lower than -0.2 is required for a 1.2 micron gap to stabilize.

The modeling work has developed a tool that allows the effects of crevice geometry and material behavior (i.e., the electrochemical kinetics of the material in the range of crevice solutions) to be predicted. The experimental work had two major aspects: (1) growth laws for crevice-corrosion damage, and (2) crevice geometry effects on crevice stability. Alloy 22 crevice-corrosion samples from the work of Kehler et al. (2001) were analyzed using the confocal microscope to quantitatively assess the extent of damage. A wide range of damage extents was included. The slope of the graph for the volume of material removed versus the maximum depth allows an assessment of the type of crevice-corrosion growth that occurred. A slope of unity indicates growth as a cylinder, a slope of two indicates trench formation, and a slope of three is consistent with growth as a hemisphere. The best fit to the data was found when a slope of one was used at small amounts of damage (<50 microns), and a slope of two was used for depths of

attack between 50 and 500 microns. Thus, it appears that the crevice corrosion in these samples started as cylinders and then evolved into trenches.

By varying the crevice gap and crevice length independently, a critical ratio of crevice gap to length was found to be required to achieve critical crevice geometry and get a sufficiently large potential drop for crevice corrosion to remain active. Thus, the solid points in Figure 2 are gap/length combinations that supported stable crevice corrosion, whereas the samples represented by the open symbols re-passivated. In addition, the standard Oldfield-Sutton model (Oldfield and Sutton, 1978) predicts that a tighter crevice gap is needed to support stable crevice corrosion than that determined in the present work. The experimental work has developed methods that can be applied to produce rigorously defined crevice geometries that allow controlled experiments to be conducted and compared to model predictions.

References

- Kehler, B.A., G.O. Ilevbare, J.R. Scully, *Corrosion*, 57 (12) (2001), 1,042, 2001.
- Oldfield, J. W., and W.H. Sutton, *British Corrosion Journal*, 13, 104, 1978.

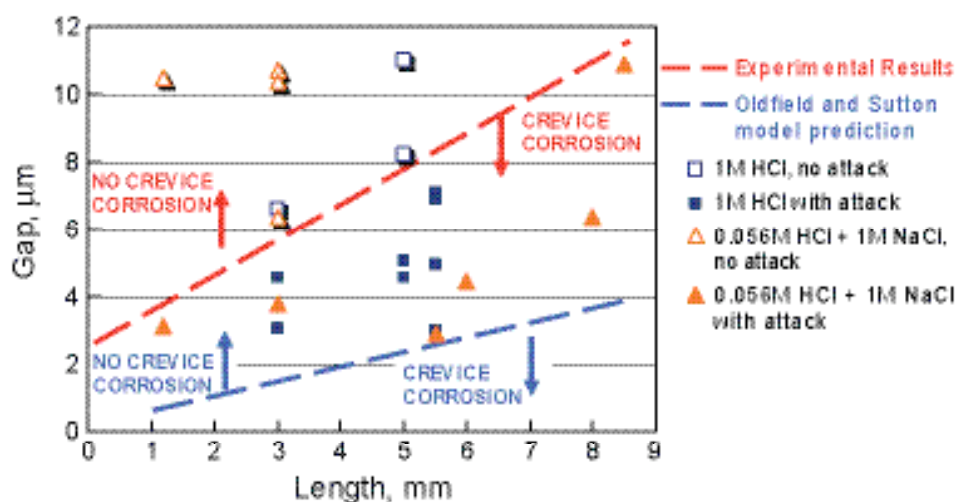


Figure 2. Crevice gap/length combinations that supported stable crevice corrosion (solid symbols), and samples for which the sample re-passivated (open symbols). Also included is the line resulting from the classical model for crevice corrosion (Oldfield and Sutton, 1978). Material: SS316L, room temperature.

Crevice-Corrosion Damage Function on Alloy 22

David W. Shoesmith, Dmitriy Zagidulin, Pellumb Jakupi, and Jamie Noël
University of Western Ontario

Research Objectives

This report presents the progress and status of the above project as part of the Materials Performance Thrust. Within the Materials Performance Thrust, leading faculty and researchers at universities and national laboratories are organized to address important issues for the long-term performance of waste package materials and other engineered materials. The primary goals of this research project are to develop a crevice-corrosion damage function that can be used to assess material penetration rates and to determine how the different alloying elements affect the crevice-corrosion resistance of Alloy 22.

Approach

Current and potential thresholds have been established to delineate the conditions required to initiate and sustain active crevice propagation in 5 M NaCl solution at 120°C. Experimental results suggest that stifling and repassivation of crevice corrosion on Alloy 22 are caused by external cathode limitations and cathodic reaction starvation.

The chemical compositions of corrosion products and corroded regions have been characterized using a variety of surface analytical techniques such as: Energy Dispersive X-ray analysis (EDX), X-ray Photoelectron Spectroscopy (XPS), and Raman spectroscopy.

Preliminary Technical Results

Initiation and subsequent crevice-corrosion propagation have been shown to be difficult on Alloy 22 under natural corrosion conditions, i.e., no applied electrochemical perturbations. Therefore the crevice corrosion of Alloy 22 was artificially initiated by a series of galvanostatic polarizations in 5M NaCl solutions at 120°C. This series of experiments showed that, independent of applied current (as long as it is large enough to initiate and maintain active crevice propagation), the measured potentials in these experiments were all shown to exceed +200 mV (in all experiments a saturated Ag/AgCl reference electrode was used) before they significantly decreased to a near-steady-state value of approximately -160 mV. This decrease in measured potential indicates the onset of

active propagation. For crevice initiation to be possible, two mandatory conditions must be satisfied – the creation of a critical chemistry, and the presence of a sufficient IR drop inside the crevice. Then, for crevices with the same tightness, higher currents will lead to shorter crevice initiation times, and for initiation and active propagation to occur, an applied current higher than 5 μA is necessary. A series of these experiments have allowed us to establish current and potential thresholds for the establishment of the necessary combination of critical chemistry and IR drop for crevice corrosion on Alloy 22 under our experimental conditions. It should be noted that this threshold current depends on a number of parameters, including solution composition, temperature, crevice tightness, etc. The potential threshold is consistent with the results from Electrochemical Impedance Spectroscopy (EIS) and XPS experiments (described in a separate technical report) which show that the threshold of ~ 200 mV vs. Ag/AgCl coincides with defect injection into the passive film, leading to a significant decrease in resistance.

Optical micrographs of the crevice-corroded regions of the Alloy 22 samples reveal the grain structure of the alloy. The grain boundaries were shown to be decorated with pits, and the grains to be partially covered with a corrosion product deposit. Closer inspection of the grain surfaces shows this deposit to be cracked and flaky. It is most likely that the grain surface was totally covered by this deposit, and that part of it was lost when it dried and fractured following emersion from solution. EDX analyses of the deposit-covered areas are dominated by Mo and W signals, whereas the composition of the uncovered areas is dominated by Ni and Cr, as expected for the alloy covered by a thin passive oxide formed on air exposure after the experiment. Under the very acidic conditions prevailing in an actively propagating crevice, Mo(VI) can create soluble compounds which become amorphous at higher pH. The surface analyses suggest that, during propagation, the surface of the grains becomes covered with such an amorphous Mo/W containing gel (which dries and cracks on emersion). It is possible that this deposited gel inhibits metal dissolution on the grain surface. Subsequent attempts to propagate corrosion in the grain boundaries may be inhibited for the same reason, leaving propagation across freshly

exposed grains as the only available route for ongoing corrosion. This could explain the observed limited propagation into the material and the much more extensive propagation across the surface.

Raman Spectroscopy analyses also showed an enrichment of Mo and W within the grain boundaries of the crevice-corroded area (Figure 1). Raman Spectroscopy data analysis (in progress) will reveal the exact Mo and

W chemistry involved (i.e., chemical bonding and oxidation states).

Therefore, the crevice-corrosion behavior in this alloy can be rationalized by considering the microchemistry imposed by the alloying elements. Moreover, additional work will be done to elucidate how the damage (penetration depth) evolves within the crevice-corroded regions with different applied propagation currents.

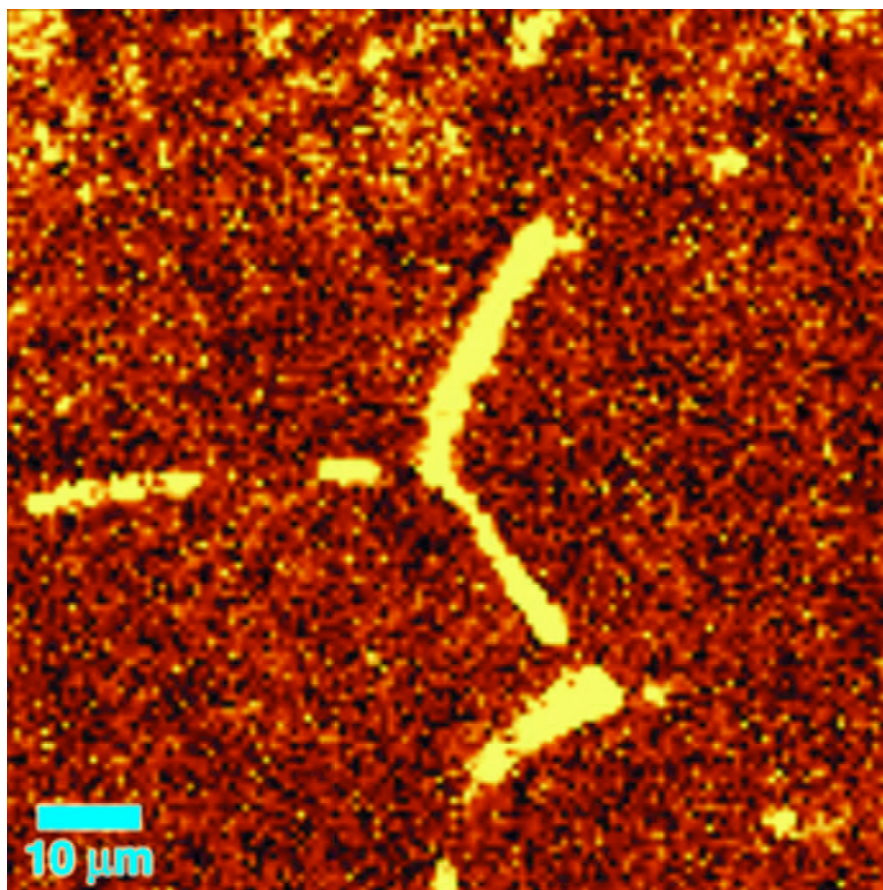


Figure 1. Raman map obtained from a crevice-corroded area. The signal intensity at each point is the integrated sum intensity for all Raman-active bands from 0 to 5,000 cm^{-1} .

Localized Corrosion Stability in the Presence of Non-Chloride Anions

Roger C. Newman and David X. He
University of Toronto

Research Objectives

This project is designed to generate rigorous electrochemical kinetic data for NiCrMo alloys in localized corrosion environments using the artificial pit technique, and then to measure and understand the effect of nitrate or other anions as inhibitors.

Approach

The artificial pit, or pencil electrode, technique involves embedding a metal wire in resin and dissolving it from one end in a salt solution, so that the entire exposed surface acquires the condition of a localized corrosion surface (pit or crevice). This creates a one-dimensional mass-transport condition while simulating the metal dissolution and solution alteration (pH, [Cl⁻]) that occur within natural localized corrosion sites. The simplified mass-transport condition enables us to determine unambiguous kinetic parameters and to study the effect of inhibiting substances such as nitrate ions.

It is important to note that with modern instrumentation, the currents that can be measured from such electrodes cover the whole range, from penetration rates of microns per second to those that are of concern for the long-term propagation of tight crevices or underdeposit events in equipment, e.g., microns per year.

The conditions chosen for the study were dilute chloride and chloride/nitrate solutions, temperature 75–95°C. A series of Ni-22Cr-xMo alloys were fabricated into thin wires and used as artificial pit electrodes.

In addition to the dc measurements, it has been valuable to use electrochemical impedance spectroscopy to measure the solution resistance within the cavity. Depending on the conditions, the ionic resistance of an anodic salt film can be measured, and the conditions for salt film formation and dissolution can be examined.

Accomplishments

There were two main aspects of the project that had to be completed. The first is the exhaustive measurement of kinetics in localized corrosion cavities; the second is the

elucidation of the effect of nitrate or other inhibitors. The nature of the first part is that not much can be published until the data are fully gathered and modeled using a finite difference procedure. We are still improving the input data (such as concentration-dependent diffusivity) that are required for this. The second aspect has shown unexpected departures from deterministic behavior that are very interesting but a little frustrating—since the *raison d'être* of the artificial pit technique is to obtain as nearly as possible deterministic behavior.

By relatively rapid back-scanning of the potential from the high-potential (diffusion controlled) condition, anodic kinetics of the alloys in the nearly saturated cavity solution were determined. These showed detailed differences from stainless steels, but nothing too surprising. Slower potential backscans allowed us to determine the response to dilution of the cavity solution. The blocking effect of alloyed Mo showed two sharp onsets: between 0 and 3% Mo, and between 9 and 13% Mo. The latter holds some interest in terms of practical considerations—the impedance study showed evidence for a resistive layer that only forms at high Mo content.

Progress has been made on the finite difference modeling of experiments where the cavity solution is allowed to dilute and the metal dissolution kinetics are measured at potentials similar to those prevailing in practice. Data have been obtained on concentration-dependent diffusivity that are essential for a properly modeled result. Surprisingly, in terms of critical concentration of pit solution, at 90°C there is not much effect of Mo content up to 9% on the repassivation condition.

In Figure 1, preliminary results for NiCr alloy show more immediate but less complete repassivation (indicated by rapid decrease of current) than 316SS on nitrate addition. This result, which has not been completely reproducible to date, is being examined. Even the 316SS shows a random element in the time to repassivation in extremely well-controlled, identical experiments. We are now working intensively on this aspect. Our hypothesis was that a 125 μm wide artificial pit electrode, apparently dissolving uniformly, still has areas of active and passive state that move around with time. Impedance data have confirmed this suggestion, even for 316SS at room temperature. So

with nitrate present, there is a stochastic aspect in the repassivation event depending on these local sites and how they are impacted, individually, by nitrate ingress. There is a feedback process such that once repassivation

starts at one site, it tends to kill dissolution on the whole electrode. This may occur by runaway nitrate reduction accompanied by solution dilution.

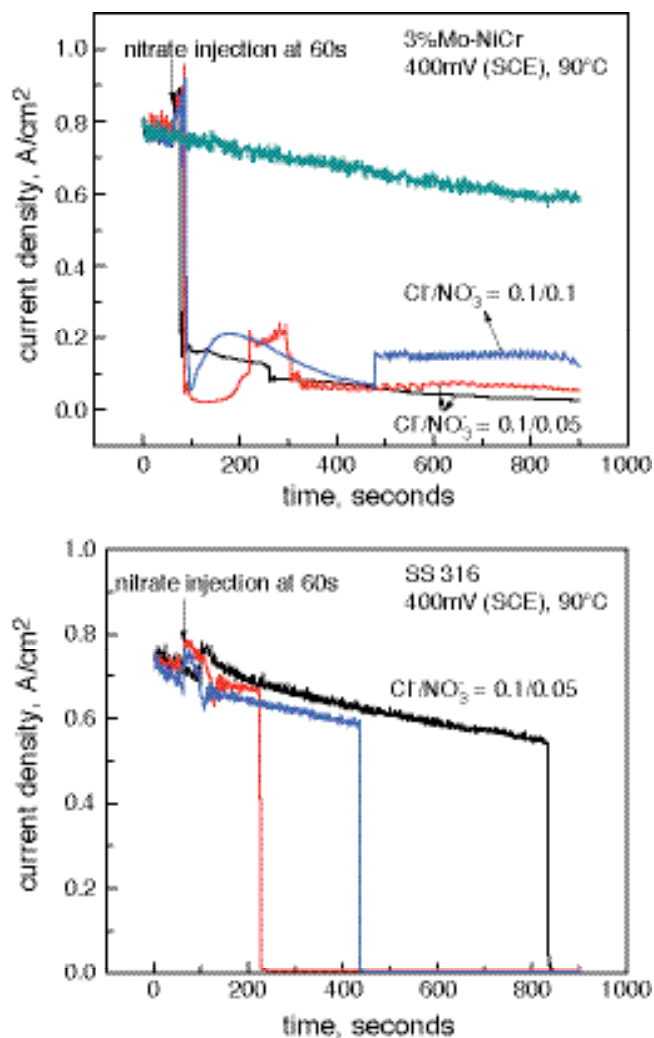


Figure 1. Current transients for Ni-22Cr-3Mo and SS316 upon injection of nitrate to the indicated molar levels after growth of an artificial pit cavity in pure 0.1M NaCl solution to ca. 400 microns depth at 90°C.

Metallurgical Effects on Localized Corrosion of Ni-Cr-Mo Alloys

Gerald S. Frankel, Rudolph G. Buchheit, Ajit Mishra, and Federico Gambina
Ohio State University

Research Objectives

The objectives of this project are to study several metallurgical aspects of localized corrosion. These could include changes produced by welding and long-term aging on the corrosion resistance of Alloy 22.

Approach

Alloy 22 is highly resistant to general and localized corrosion. However, in aggressive conditions of high chloride concentration, applied potentials, and temperature, it may suffer crevice corrosion, a form of localized corrosion. The effects of a variety of factors, including metallurgical factors, on localized corrosion are being studied. Cyclic potentiodynamic polarization (CPP) is a common technique for the assessment of localized corrosion in metallic alloys. However, the standard CPP methodology does not determine a conservative value of repassivation potential ($E_{R,CREV}$) because the pit or crevice does not grow deep. A novel approach named the Tsujikawa-Hisamatsu Electrochemical (THE) technique is being used to assess crevice corrosion in Alloy 22, because it provides a more conservative value of $E_{R,CREV}$. One aspect of the current study is to assess the procedures used in the THE technique. The revised procedure has been used to study welded and nonwelded Alloy 22 and to evaluate the influence of various oxyanion species in solution. Oxyanions like nitrates can act as inhibitors of Alloy 22 corrosion in the presence of chloride.

Accomplishments

The standard definition of Crevice Repassivation Potential ($E_{R,CREV}$) in the THE technique is “the potential in step 3 where the current density does not increase with time and also not afterward,” shown as $E_{R,CREV}(I)$ in Figure 1. In many cases, the assignment of this value is unclear because the current can increase again at lower potentials, indicating that crevice corrosion had not repassivated. This suggests that the first definition does not provide a conservative estimate of repassivation potential. In this work, a new definition of $E_{R,CREV}$ has been evaluated.

$E_{R,CREV}(II)$ in Figure 1 is the potential at which the cur-

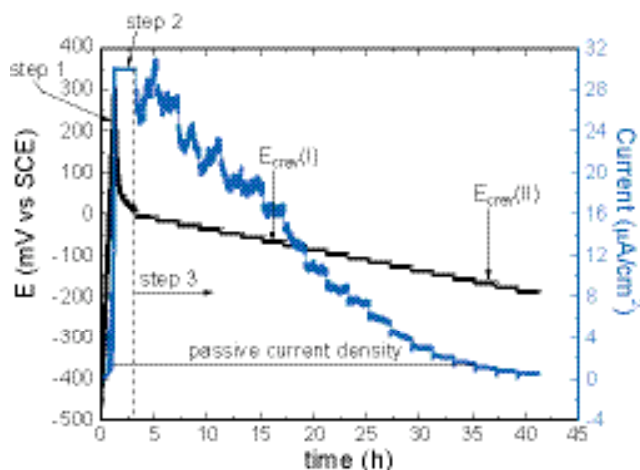


Figure 1. Schematic of THE technique showing different steps.

rent density reached the passive current density measured on the upward scan.

The difference between $E_{R,CREV}(I)$ and $E_{R,CREV}(II)$ is small (about 10 mV) when the hold current density in Step 2 is small, $2.1 \mu\text{A}/\text{cm}^2$. However, for a hold current density of $30 \mu\text{A}/\text{cm}^2$, $E_{R,CREV}(II)$ is 75–100 mV lower and much more reproducible. Thus, the newer definition of crevice repassivation potential in the THE technique is better because it is more conservative and reproducible. Further, $E_{R,CREV}(II)$ for bulk and welded Alloy 22 specimens at 90°C is within 5–10 mV, indicating that the weld has similar susceptibility to crevice corrosion as the base metal. It should be noted that the passive current density measured on the upward scan might not be an accurate reflection of the true passive current density on the backwards scan, which is expected to be somewhat lower as a result of the excursion to higher potential. Nonetheless, the potential at that current density measured during the backscan is a figure of merit that provides a reproducible value.

The change in the definition of $E_{R,CREV}$ enabled a change to the procedure for the THE technique that makes the test easier and faster. The potentiostatic steps in Step 3 were replaced by a potentiodynamic sweep at a scan rate of 0.167 or 0.0167 mV/s. The values of $E_{R,CREV}(II)$ were found to be relatively independent of scan rate at 75 and

90°C and in 0.1 and 1.0M NaCl, and were similar to the values determined by the standard potential stepping approach.

The modified THE procedure was used to investigate the inhibitive effects of various oxyanions such as nitrate, sulfate, carbonate, and bicarbonate. A critical value of the ratio $\text{NO}_3^-/\text{Cl}^-$ was found for complete inhibition of crevice corrosion. When $\text{NO}_3^-/\text{Cl}^- > 0.2$ at 90°C, the apparent repassivation potential jumped by hundreds of mV, and no crevice corrosion was observed (Figure 2).

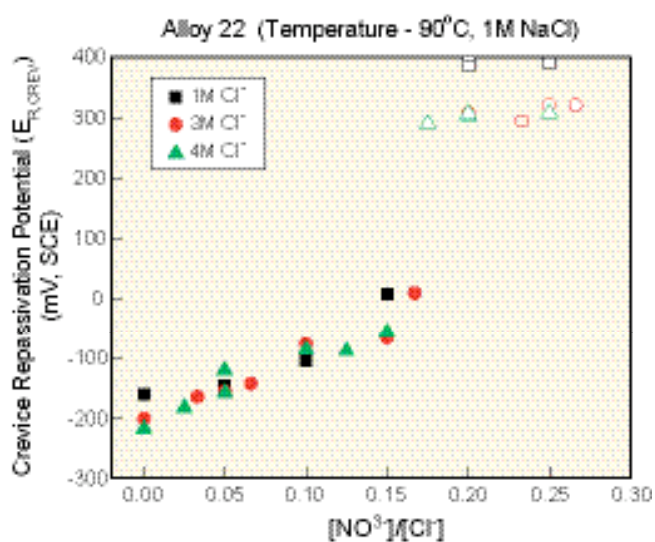


Figure 2. Effect of nitrate ions on inhibition of crevice corrosion of Alloy 22 in aggressive solution (open symbol indicates no crevice attack).

Addition of sulfate in a chloride environment also resulted in inhibition of crevice corrosion of Alloy 22, but a much higher concentration was needed. At 90°C, the critical

$\text{SO}_4^{2-}/\text{Cl}^-$ ratio for complete inhibition was 1.5 at 1.0 M Cl^- and 0.6 at 0.1 M Cl^- .

Interestingly, the amount of nitrate required for complete inhibition of crevice corrosion of Alloy 22 decreased slightly when sulfate was added to the chloride solution. Further, there was no negative effect of sulfate addition (both at high and low sulfate concentration) to nitrate inhibition in a chloride environment at high temperature. Thus, it can be concluded that the concentration of strong inhibitor needed for complete inhibition of crevice corrosion of Alloy 22 in an aggressive environment decreased slightly when mixed with a weak inhibitor. Current work is investigating the effect of other inhibitive anions like carbonate and bicarbonate (individually and mixed) on the inhibition of crevice corrosion for Alloy 22 in an aggressive environment.

The THE technique was modified further to determine crevice repassivation temperature, $T_{R,CREV}$. In this new approach, the first two steps were identical to the standard THE technique, as shown in Figure 1. However, the third step consisted of holding the potential constant and decreasing the temperature stepwise, 2°C every 20 min. The current was monitored with time, and the temperature at which the current density in Step 3 reached the passive current density that was measured on the upward scan is defined as $T_{R,CREV}$. This experiment was performed in 1M NaCl solution at a hold current density of 3 or 7 $\mu\text{A}/\text{cm}^2$, and the initial temperature in Step 3 was 90°C, for both bulk and as-welded Alloy 22 specimens. $T_{R,CREV}$ was around 69 and 65°C for unwelded and welded Alloy 22, respectively. $T_{R,CREV}$ was not strongly influenced by the hold current density for both bulk and as-welded Alloy 22 specimens. The lower $T_{R,CREV}$ for the welded alloy indicates a slightly increased susceptibility to crevice corrosion.

Processes in Crevice-Corrosion Propagation, Stifling, and Arrest

Joe H. Payer, Xi Shan, Arun S. Agarwal, and Uziel Landau
Case Western Reserve University

Research Objectives

The objective is to analyze crevice-corrosion-damage evolution for passive metals covered by layers of moisture, particulate, and deposits. A focus is the determination of the effect of the crevice former on localized corrosion damage propagation. In accelerated tests, crevice corrosion is forced to initiate by aggressive environments and applied potentials. Then, the post-initiation stages of propagation, stifling, and arrest are examined. Computational analysis of the creviced area is conducted for evolution of corrosion damage by modeling of the current flow and potential gradients coupled to process chemistry and electrochemistry.

Approach

Our approach consists of a combination of experimental measurements of localized corrosion with various crevice formers, and analytical computations of the crevice damage profile as a function of crevice geometry, environment, and corrosion resistance of the metal. Standard crevice corrosion test methods are modified by (a) the use of metal, polymer, and ceramic materials as crevice formers and (b) the variation in size and shape of the crevices. The metal surface, deposits, and corrosion products are analyzed. Further post-test analysis includes 3-D reconstruction of corrosion damage profiles. Figure 1 shows the crevice test assembly, a crevice former, and post-test crevice-corrosion damage.

Accomplishments

Stages of Crevice Corrosion Damage Evolution

During constant potential tests, measurements of the current indicate the initiation and rate of crevice corrosion through the stages of propagation and any stifling or arrest. Four stages of crevice corrosion have been observed: initiation, propagation, stifling, and arrest. Typical results are shown in Figure 2. In many cases, after an incubation period the corrosion current increased, and then a number of stifling steps (decreased current) were observed followed by arrest (repassivation). The onset of crevice corrosion, the amount of damage observed, and the occurrence of sti-

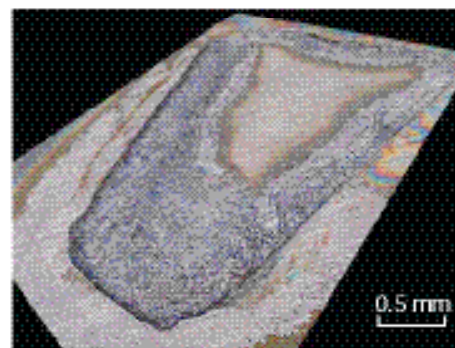
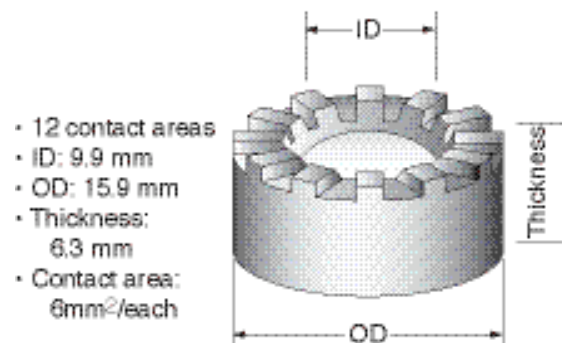


Figure 1. (a) A multi-crevice test assembly, (b) a schematic of the crevice former (12 contact areas) and (c) post-test micrograph of corrosion damage beneath one crevice contact area after an accelerated test.

fling or arrest depend upon the severity of the test conditions. Tests were interrupted after different levels of damage in order to examine damage evolution. Surface profiles after different amounts of damage (coulombs of corrosion) are shown in Figure 3.

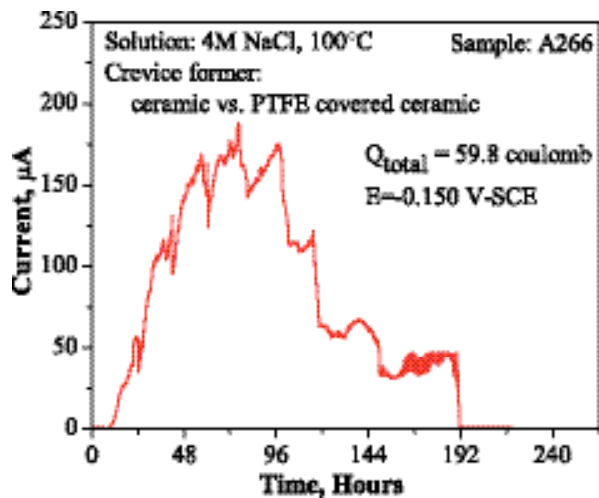


Figure 2. The current in constant potential tests indicates the initiation (current rise) and rate of corrosion throughout the test. Drops in current indicate stages of stifling and arrest of corrosion.

Effect of Crevice Former on Localized Corrosion

A necessary condition for crevice corrosion is that a crevice former must create a restricted geometry on the metal surface. Crevice corrosion is affected by the crevice geometry and properties of the crevice former. An important issue is how effective particulate layers and deposits are as crevice formers compared to metal/metal crevices and polymer/metal crevices used in laboratory tests. In head-to-head comparisons, the polymer-covered ceramic crevice former (an accelerated laboratory technique) was significantly more severe than a ceramic or a polymer alone.

Analysis of Corrosion Products and the Alloy Surface after Corrosion

For Alloy 22 (Ni-Cr-Mo-W alloy), the metal surface

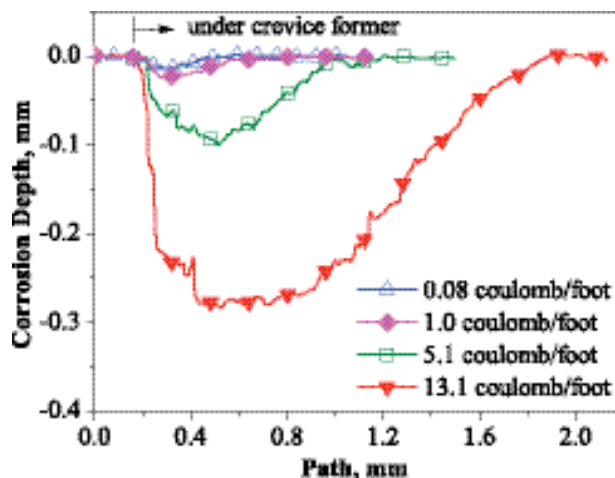


Figure 3. Corrosion damage profiles after different amounts of damage (coulombs of corrosion). The damage profiles indicate deepest penetration toward the outer edge of the contact area (foot) and propagation across the contact area.

beneath corrosion products had essentially the same composition as the bulk alloys, indicating congruent dissolution. The passive film under the corrosion products was a chromium oxide-type as is found on the bulk alloy. Corrosion products within the crevice area were enriched in Mo and W, two elements that increase the corrosion resistance of the alloy. The Ni was found to transport as a soluble ion from the crevice to the solution outside of the crevice.

This project addresses factors that affect the initiation, propagation, stifling, and arrest of localized corrosion. The findings are an important contribution to the determination of the penetration rate and extent of corrosion damage by localized corrosion over extremely long times.

Combinatorial Chemistry Approaches for Alloy Composition and Corrosion Behavior

Rudolph G. Buchheit, Gerald S. Frankel, and Fariaty Wang
Ohio State University

Research Objectives

The objective of this project is to study the effect of alloy composition on the corrosion behavior of Ni-Cr-Mo alloys. The role of each alloying element was examined by analyzing the electrochemical response for different temperatures and solution chemistries. Correlation of alloy composition to localized corrosion behavior was constructed using multiple linear regression analysis on the electrochemical data collected.

Approach

Ni-based solid solution alloys with variations in Cr (8 to 30% by weight) and Mo (3 to 25% by weight) content were fabricated using vacuum arc melting. The fabricated alloys were heat treated to develop more homogenized microstructure.

Electrochemical characterization was performed using a Multichannel Microelectrode Analyzer (MMA) (Scribner Associates, Inc., Southern Pines, NC). The MMA allows simultaneous measurement of multi-element working electrode arrays. Arrays used in this study were comprised of the different alloy compositions fabricated. Anodic and cathodic polarization curves were collected using this approach. Little variation in cathodic polarization behavior as a function of alloy chemistry was detected, and experiments have focused on composition dependence in the anodic polarization response. Anodic polarization measurements were carried out using dilute and acidified chloride solutions with temperatures ranging from 45 to 90°C.

Characteristic potentials (corrosion potential E_{corr} , critical pitting potential E_{pit} , transpassive potential E_{tr} , and repassivation potential E_{repass}) extracted from the anodic responses of the Ni-Cr-Mo alloys in dilute sodium chloride solutions at various temperatures were used in multiple linear regression analysis, in order to relate their variation to alloy composition. The validity of these expressions was tested by comparing to characteristic potentials of the same Ni-Cr-Mo alloys measured in acidified chloride, sul-

fate, and nitrate solutions at various elevated temperatures.

Accomplishments

Anodic polarization response of the alloys in a warm to hot dilute sodium chloride solution shows that alloys with low Cr and Mo experienced pitting. Alloys with very low Cr content (about 10 wt.%) suffer severe corrosion that looks more like uniform rather than localized corrosion,

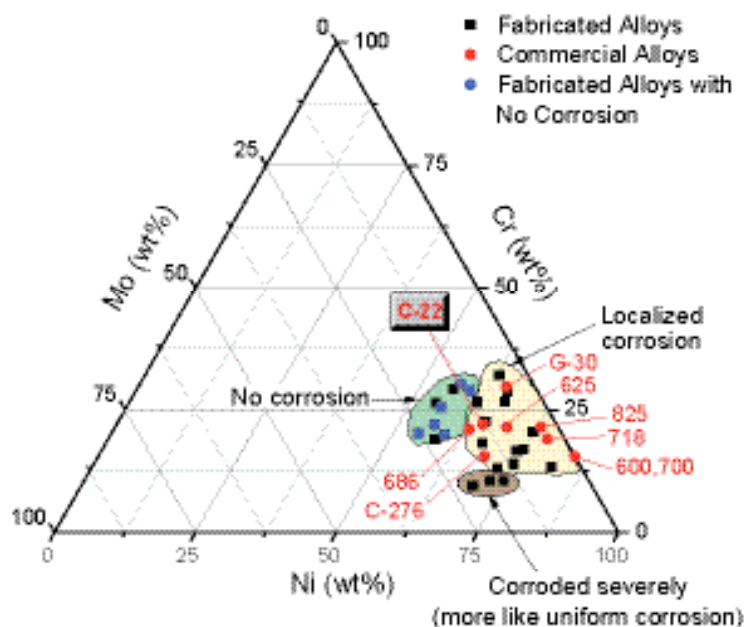


Figure 1. A Ni-Cr-Mo ternary diagram showing composition regions of alloys that experience severe uniform corrosion, localized corrosion, or are corrosion resistant.

while some alloys with moderate to high amount of Cr and Mo demonstrated high resistance to localized corrosion. The most corrosion resistant alloys have Cr content between 20 to 30 wt. % and Mo content between 12 to 25 wt. %. Figure 1 is a Ni-Cr-Mo ternary diagram showing regions of alloying composition that exhibited localized corrosion, susceptibility to severe (more uniform) corrosion, and corrosion resistance. Alloy 22 is close to the no-corrosion region. However, it should be noted that the effects of tungsten, iron, and other alloying elements in

Alloy 22 are not accounted for in this study.

Multiple linear regression analysis is performed on these anodic polarization data sets. The correlations between the breakdown potential (E_b) and repassivation potential (E_{rp}) with Cr and Mo content at different temperatures are shown in Table 1. It is observed that the role of Mo has become more significant as the temperature increases, as seen by the increasing Mo/Cr ratio in Table 1, particularly on the repassivation potential. The correlation factor for the breakdown potential at 45°C is low, because most alloys did not experience breakdown in that mild environment. Synergistic effects between elements have not been evaluated.

Anodic polarization measurements were also performed on the same Ni-Cr-Mo alloys in pH 2.75 mixed chloride-sulfate and nitrate solutions at 60, 80, and 95°C. Similar to the dilute sodium chloride experiments, the alloys

that show high resistance to breakdown are alloys with 20 to 30 wt.% Cr and 12 to 25 wt.% Mo. It is noted that there is a regular dependence between the breakdown potential estimated from the correlation equations from Table 1 and the experimental data. There is some dependency on the repassivation potential from the correlation equation to the experimental data, although it is less regular than the breakdown potential.

In stainless steels, Pitting Resistance Equivalency Number (PREN) is often used to rank pitting susceptibility based on the content of the alloying elements. Table I suggests that the correlation between alloy composition and localized corrosion behavior of Ni-Cr-Mo alloys is considerably different than that of stainless steels. As such, the PREN expression developed for stainless steels should be used with caution when assessing tendencies for localized corrosion of Ni-Cr-Mo alloys.

Table I. Equations that correlate breakdown (E_b) and repassivation potentials (E_{rp}) to Cr and Mo content obtained from multiple linear regression analysis on experimental data

Temp (°C)	Fitting Results	R ²	Mo/Cr
45	$E_b = 0.77(\text{wt}\% \text{Cr}) + 1.16(\text{wt}\% \text{Mo}) + 558.44$	0.57	1.5
60	$E_b = 7.95(\text{wt}\% \text{Cr}) + 12.99(\text{wt}\% \text{Mo}) + 133.82$	0.92	1.6
75	$E_b = 10.09(\text{wt}\% \text{Cr}) + 15.24(\text{wt}\% \text{Mo}) + 37.49$	0.85	1.5
90	$E_b = 7.79(\text{wt}\% \text{Cr}) + 18.69(\text{wt}\% \text{Mo}) - 26.5$	0.83	2.4

Prediction of the Time Evolution of Localized Corrosion Damage

Digby D. Macdonald, Igor Nicić, and George R. Engelhardt (Consultant)

Pennsylvania State University

Research Objectives

The purpose of this project is to further identify the important electrochemical processes and parameters involved in long-term corrosion. More specifically, the project purpose involves development of theoretical models, use of electrochemical measurements, and calculating long-term evolution of corrosion damage.

Approach

Both theoretical and experimental studies are under way to address the understanding of long-term corrosion prediction.

Chronoamperometry experiments have been performed on Type 316L stainless steel, and the transition from metastable pitting to stable pitting was observed, showing that 316L SS does exhibit typical pitting characteristics that have been observed for many other stainless steels. The purpose of this work was to experimentally determine the survival probability, which is the ratio of number of metastable pits that occur before a transition to a stable pit is observed, divided by the total number of metastable events. It is expected to be a function of $[Cl^-]$, potential, pH, temperature, etc.

An artificial pit has been developed and used to study the effect of pit depth on the “observed” critical breakdown potential. The artificial pit can also be used to study the separation of anodic and cathodic reactions and to understand how the length of the diffusion path affects the pit growth and repassivation.

Passivity breakdown is the initial event that occurs in the nucleation of localized corrosion damage. Accordingly, a viable mechanistic description of this phenomenon is important for the development of deterministic models for predicting the evolution of localized corrosion damage on metal and alloy surfaces. (Macdonald, 1999; Macdonald and Urquidi-Macdonald, 1992). One interesting observation is that most if not all metals and alloys display susceptibilities towards passivity breakdown that depend on anion size. Thus, for the stainless steels, iron, and nickel, the ability of halide ions to induce passivity breakdown lies in the order $F^- < Cl^- > Br^- > I^-$, whereas in the case of

titanium, the greatest susceptibility is induced by bromide ion. These observations suggest that ion size is an important, but not the sole, factor in determining the ability of an anion to induce passivity breakdown. This is because, while ion size changes monotonically along the halide series, the ability of the halide to induce passivity breakdown passes through a maximum.

The anion size effects on passivity breakdown are explored theoretically within the framework of the Point Defect Model (PDM). It is shown that the observed dependence of the breakdown potential on anion size can be accounted for at a semi-quantitative level by the PDM in terms of three factors that affect the absorption of the halide into surface oxygen vacancies: (1) the work of expansion of the vacancy to accommodate the adsorbing halide ion, (2) the accompanying entropy change, and (3) dehydration of the anion and possibly also of the surface oxygen vacancy. All three of these factors control the thermodynamics of anion absorption into a surface oxygen vacancy, but the impact that each has on the Gibbs energy of absorption occurs in opposite directions as the anion radius is changed. Thus, increasing ion size requires greater work to be performed in expanding the vacancy to accommodate the ion and hence gives rise to an increasingly positive contribution to ΔG . Contrariwise, increasing anion size gives rise to a smaller positive contribution to ΔG from the change in entropy and to a less positive Gibbs' energy change for anion dehydration. These factors cause the Gibbs energy of adsorption to pass through a positive minimum as a function of ion size. For the passive films on iron, nickel, and stainless steels, the extremum in ΔG occurs roughly at the ionic radius of Cl^- . Increasing the size of the oxygen vacancy results in a shift in the contribution to ΔG from vacancy expansion to larger ionic radius, so that the minimum in ΔG shifts in like manner. This effect is offered as the explanation as to why bromide ion is most aggressive in the case of passivity breakdown on titanium, whereas chloride is most aggressive in the case of iron, nickel, and the stainless steels, assuming that an oxygen vacancy in the surface of the passive film on titanium is larger than in the surface of the barrier layer on iron (or nickel). However, complete theoretical resolution of these effects will require careful definition of the sizes of surface oxygen vacancies in the barrier passive films on various metals and alloys.

Two problems regarding theoretical treatment of the accumulation of corrosion damage inside the crevice have been considered. First, we considered the accumulation of chloride or other aggressive anions inside the crevice, due to the establishment of a differential aeration cell. Second, we considered the development of a preliminary version of a code for deterministic Monte Carlo simulation of corrosion damage. Relative to the first problem, our main aim was to develop a relatively simple method for predicting the chloride concentration, pH, and potential distribution inside an active crevice. The current density inside pits, i_{pit} (i.e., the rate of pitting corrosion) can be described in general terms by the equation:

$$i_{pit} = k_A C_A^\lambda$$

where C_A is the concentration of the aggressive anions, k_A is the rate constant for the reaction proceeding in the anodic direction (which depends on potential and, in the general case, on pH), and λ is the effective kinetic order of the metal dissolution reaction with respect to the anion concentration. In many cases, the value of λ is between 0.5 and 1, which indicates that this dependence can be important. In addition, information about $[Cl^-]$ is critical for predicting breakdown with the PDM, as this is the value that determines the passivity breakdown voltage and the rate of pit nucleation (MacDonald and Urquidi-Macdonald, 1987; 1989; 1992).

Experimental electrochemical impedance studies (EIS) and Mott-Schottky analysis of 316L SS have been performed to further validate the PDM. 316L SS was chosen because its passive film is primarily defective chromic oxide, which is the same as in Alloy 22, and because it is much more prone to corrosion than Alloy 22. The solution used was 0.2M borate buffer with the pH of 8.35. As a part of extracting kinetic parameters from impedance data, a code was developed.

Accomplishments

1. We evaluated the impact of $[Cl^-]$ and potential on the survival probability and reported the preliminary results.
2. We showed that the observed dependence of the breakdown potential on anion size can be accounted for at a semi-quantitative level by the PDM in terms of three factors that affect the absorption of the halide into surface oxygen vacancies.
3. We developed a simplified and very accurate analytical method for estimating chloride concentrations and potentials inside the crevice. It has been shown that the amplification factor for the chloride concentration is proportional to the passive corrosion current density and to the square of the crevice depth, and it is inversely proportional to the width of the crevice and to the chloride ion bulk concentration. Also, it has been shown that the influence of the external environment must be taken into account to quantitatively describe the transport processes inside the crevice.
4. We developed a preliminary model for Monte Carlo simulation of pitting corrosion damage inside the crevice.
5. We developed a code enabling us to perform non-linear regression while imposing constraints on the parameters to be optimized, as well as applying the most appropriate weighting functions to the EIS data.

References

- Macdonald, D.D., *Pure Appl. Chem.*, 71, 951, 1999.
Macdonald, D.D., and M. Urquidi-Macdonald, J. *Electrochem. Soc.*, 134, 41, 1987.
Macdonald, D.D., and M. Urquidi-Macdonald, J. *Electrochem. Soc.*, 136, 961, 1989.
Macdonald, D.D., and M. Urquidi-Macdonald, J. *Electrochem. Soc.*, 139, 3434, 1992.

EVOLUTION OF MOISTURE ENVIRONMENT ON METAL SURFACES

Modeling Chemical Environments within Corroding Crevices for Ni-Cr-Mo Alloys

Peiming Wang, Ronald D. Springer, and Andre Anderko, OLI Inc.

Evolution of Solution Layer Chemistry during Localized Corrosion

Robert G. Kelly and Z. Chen, University of Virginia

Modeling and Measurement of Current Distribution on Particulate and Deposited Layers

Uziel Landau, Arun S. Agarwal, Xi Shan, and Joe H. Payer
Case Western Reserve University

Microelectronic and MEMS Devices for Solution Properties and Corrosion Evaluations

Chung-Chiun Liu, Meijun Shao, and Laurie Dudik, Case Western Reserve University

Optical Probes and Sensors to Determine Concentration Distributions in Thin Films on Reactive Surfaces

William H. Smyrl and Francis Guillaume, University of Minnesota

High-Temperature Multi-Species Solution Properties and Behavior

David R Cole, Lawrence M. Anovitz, Mirosław S. Gruszkiewicz, Donald A. Palmer, Jorgen Rosenqvist, David J. Wesolowski, and Leslie L. Wilson, Oak Ridge National Laboratory; Lawrence M. Anovitz, University of Tennessee; Andre Anderko, George Engelhardt, and Peiming Wang, OLI Systems; Digby D. Macdonald, Pennsylvania State University

This page intentionally left blank.

Modeling Chemical Environments within Corroding Crevices for Ni-Cr-Mo-W-Fe Alloys

Peiming Wang, Ronald D. Springer, and Andre Anderko
OLI Systems Inc.

Research Objectives

The objective of this project is to develop a comprehensive model for the thermophysical properties of the environments that are likely to occur within corroding crevices in Ni-Cr-Mo-W-Fe alloys. Such a model is an important component for understanding the propagation, stifling, and inhibition of crevice corrosion.

The environments within actively growing crevices contain chloride solutions of dissolved metal species whose concentrations may reach or approach saturation. Further, the solutions are usually strongly acidic because of hydrolysis of metal cations, which drives the pH below the depassivation pH of the alloy. Thus, quantitative modeling of environments within growing crevices necessitates a comprehensive treatment of dissolution products of Ni, Cr, Mo, W, and Fe in acidic chloride solutions. Further, it is necessary to account for the effects of other common anions that may coexist with chlorides, especially sulfates and nitrates. The main properties of interest here are (1) the solubilities of various solid corrosion products, which provide the limits of concentrations in the anodic environment; (2) speciation of the solution, i.e., the chemical identity and distribution of species including products of hydrolysis and complexation; (3) activities of dissolved species, including the effective solution pH; (4) diffusivities and ionic conductivities of individual species, and (5) overall properties of the anodic solution, including ionic conductivity and density.

Approach

Previously developed models have been shown to be capable of reproducing thermodynamic and transport properties of mixed-solvent electrolyte (MSE) systems in wide ranges of concentration and temperature. The MSE thermodynamic model has been shown in previous studies to be very accurate for representing the properties of complex, multicomponent salt solutions in wide concentration ranges (i.e., up to the fused salt or solid saturation limit). Therefore, it has been selected for modeling the properties of chemical environments that exist within the crevice as well as those outside of the crevice. Recently, it has been successfully applied to model deliquescence in Na-K-Mg-Ca-Cl-NO₃ systems.

In this work, we developed a self-consistent set of parameters for the Ni-Cr-Mo-W-Fe-H-Cl-SO₄-NO₃ systems. The work was focused on the following tasks:

- (1) Literature search and critical evaluation of thermodynamic and transport property data for aqueous Ni-Cr-Mo-W-Fe-H-Cl-SO₄-NO₃ mixtures. The data include phase equilibria, speciation data from spectroscopic and other measurements, pH data, heats of dilution and mixing, densities, diffusion coefficients, viscosity, and electrical conductivity. These data allow us to constrain thermodynamic and transport parameters to obtain a self-consistent model of crevice chemistry.
- (2) Development of thermodynamic parameters of the MSE model for systems containing Ni(II), Fe(II), Fe(III), Cr(III), Mo(III), Mo(IV), Mo(VI), and W(VI) in neutral and acidic solutions containing chlorides, nitrates, and sulfates.
- (3) Development of parameters for associated transport-property models. Specifically, electrical conductivity and self-diffusivity model parameters have been developed for aqueous chloride, nitrate, and sulfate solutions of Ni(II), Fe(II), Fe(III), and Cr(III), and for neutral and acidic solutions of Mo(VI) and W(VI). Transport property model parameters have been developed based on the speciation obtained from thermodynamic equilibrium calculations.

Attention was focused on the properties of relevant salt subsystems and mixtures containing both salts and corresponding acids. This treatment ensured that the model realistically reproduces the crevice environments, which are acidic during the propagation of localized corrosion.

Accomplishments

Thermodynamic and transport property data have been successfully reproduced for the following classes of systems:

- (1) Chlorides, sulfates, and nitrates of chromium (III),

nickel (II), and iron (II and III)

- (2) Systems combining the metal chlorides, sulfates, and nitrates with hydrochloric, sulfuric, and nitric acids
- (3) Molybdenum (III, IV, and VI) and tungsten (VI) oxides and their mixtures with hydrochloric, sulfuric, and nitric acids.

Because of the predictive nature of the model, accurate reproduction of the properties of the above systems ensures the correct representation of the properties of mixed Ni-Cr-Mo-W-Fe systems. This has been demonstrated using available data for the dissolution of alloys including both pH values and solubility limits.

Figure 1 illustrates the representation of pH data in systems containing Cr(III) ions. The agreement with experimental data indicates that the hydrolysis of ions is accurately reproduced. Figure 2 shows the calculated and experimental solubilities of WO_3 in HCl and HNO_3 . As shown in the figure, the Cl^- and NO_3^- ions have a markedly different effect on the solubility of WO_3 at higher acid concentrations, which can be expected to correlate with the behavior of passive films.

The MSE models for thermodynamic and transport properties have been implemented in a general software system.

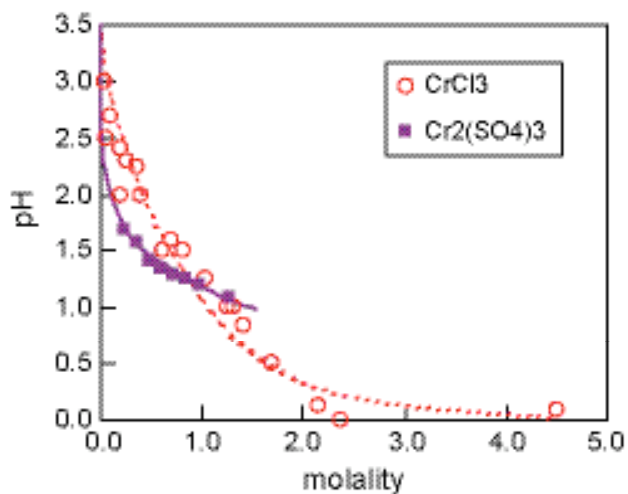


Figure 1. Comparison of calculated and experimental pH values for $CrCl_3$ and $Cr_2(SO_4)_3$ solutions. The data are from Mankowski and Szklarska-Smialowska (*CorrSci* . 1975, 15, 493) and Vinokurov et al. (*RussJCoordChem* . 2004, 30, 496).

Coupled with a graphical user interface, the software can be used to calculate all the necessary thermodynamic and transport properties. Alternatively, a callable module can be used to provide thermophysical properties to other higher-level programs. The callable version can be used as a phase equilibrium and thermophysical property generator for programs that model the evolution of crevice corrosion.

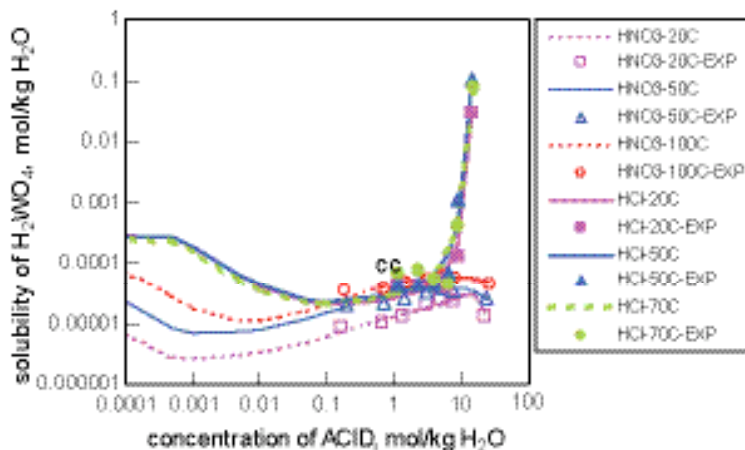


Figure 2. Comparison of the effects of chloride and nitrate ions on the solubility of W(VI) oxide in acidic solutions. The thick lines indicate a steep increase in solubility as a function of Cl^- concentration, whereas a weak decrease is observed for NO_3^- ions. The data are from Meerson and Mikhailova (*RussJInorgChem* . 1967, 12, 849) and Wood (*Geochim Cosmochim. Acta* 1992, 56, 1827).

Evolution of Solution Layer Chemistry in the Presence of Dust

R. G. Kelly and Zhuoyuan Chen
University of Virginia

Research Objectives

The goal of this study is to investigate the ability of a wetted metal surface of limited area to support an active localized corrosion site via the production of cathodic current. Studies of cathodic control of localized corrosion of corrosion-resistant alloys are sparse, and studies considering thin electrolyte layers are essentially nonexistent. Quantification of the total current that a wetted surface could deliver under a given set of conditions provides a scientific basis for analyses of both the maximum rate and the stability of localized corrosion. These results will be coupled with complementary calculations of the requirements of localized corrosion sites for current to remain stable.

Approach

An analytical method for evaluating the stability of pitting corrosion of corrosion-resistant alloys under thin-layer conditions was sought. The method utilizes the concept of an equivalent cathode (Chen et al., 2007; Chen and Kelly, 2007) to calculate the maximum cathodic current, termed the cathode capacity, that can be provided by a surface exposed to a given set of atmospheric conditions, i.e., temperature, relative humidity (RH), and deposition density of salt. Knowledge of the geometry of the cathode and its electrochemical kinetics are needed as input, as is deliquescence data for the salt of interest.

The anode demand (the minimum current required to maintain stability in a localized corrosion site) can be calculated via the Galvele pit stability criterion, and depends on the localized corrosion site geometry and the pit stability product, which is a material property. By coupling these two approaches, the stability of a pit or other localized corrosion site can be determined for a given environmental scenario. The method has been applied to the atmospheric pitting corrosion of Type 316L stainless steel, leading to a quantitative description of limiting stable pit sizes.

Accomplishments

The analytical equations developed for both one- and two-dimensional geometries have been validated against finite element calculations. The equations have then been exer-

cised for a variety of atmospheric scenarios to develop quantitative descriptions of the total cathode current available. Figure 1 shows an example for Type 316L stainless steel. For a circular cathode surrounding a circular pit, a linear dependence of the total cathode current on the deposition density was found. In addition, the total cathode current increases with increasing pit size due to the decrease in the approach resistance for a larger pit. This effect allows a larger cathode area to participate.

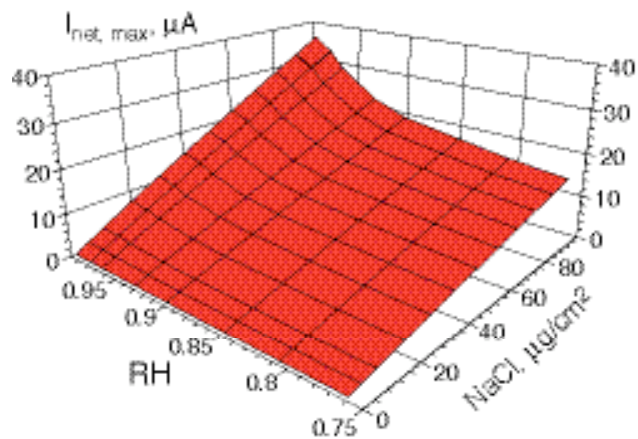


Figure 1. The effect of relative humidity and amount of deposited NaCl particles on the cathode capacity of SS 316L under atmospheric exposure. The cathode is circular around a pit with radius of 10 μm . Temperature is 25°C.

The coupling of the cathode capacity equations to a localized corrosion site stability criterion is shown in Figure 2 for several scenarios. At high RH and deposition density, the cathode capacity curve (I_{net}) exceeds the anode demand (I_{LC}) for pit sizes below 39 microns. Thus, pits below this size can grow stably. However, once a pit reaches 39 microns, it can no longer grow with the cathode being considered. It must either fully repassivate or stifle in such a way that only a portion of its surface remains active.

If the RH is lowered to 85%, the maximum stable pit size decreases to less than 20 microns; similarly, if much of the salt were washed off, the maximum stable pit size falls to below 10 microns. Under these conditions, previously

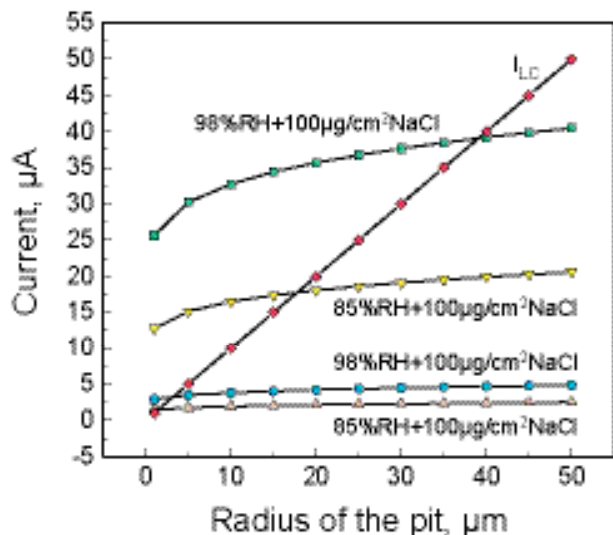


Figure 2. The effect of the radius of the pit on the circular cathode capacity, $I_{net, max}$, and anodic current demand, I_{LC} . Material: 316L, room temperature.

grown pits would be unable to continue to grow, and the driving force for repassivation would be very high.

One strength of the analytical modeling is its dependence on data that are straightforward to obtain for a given exposure scenario. A great deal of salt deliquescence data exists, and generation of new data is straightforward. The cathodic kinetics can be measured in the solutions expected under full immersion conditions, with the increased oxygen reduction current experienced under thin-film conditions taken into account. Finally, the pit stability product has been determined for some materials, and the methods to do so for others are established.

A second strength of the approach is the fact that it provides a bounding estimate of total cathodic current, in the sense that a given cathode cannot produce more current than that calculated. The assumptions inherent in the calculation are that (1) the chemistry and kinetics are fixed, (2) the thin film solution has no particulate in it, and (3) the cathode surface is perfectly wetted. In reality, the pH at cathode sites rises with time from a near-neutral starting solution, and the cathodic kinetics then slow. In most engineering applications, there is dust and other particulate that would tend to increase resistivity, thereby reducing the I_{net} because more voltage is lost to ohmic drop. Finally, any contact angle less than 180° would lead to less cathode area available to supply current.

Thus, this work provides a framework for evaluating the effects of both material and environmental parameters on the bounding conditions for localized corrosion stability.

Related Publication

- Chen, Z.Y. F. Cui, and R.G. Kelly, Computational modeling of the stability of crevice corrosion of wetted SS316L. ECS Transactions (in press), 3, 2007.
- Chen, Z.Y., and R.G. Kelly, An analytical modeling method for calculating the maximum cathode current deliverable by a circular cathode under atmospheric exposure. In: Simulation of Electrochemical Processes II., V.G. DeGiorgi, C.A. Brebbia, and R.A. Adey, eds., WIT Press, Boston, pp. 33-42, 2007.
- Payer, J. H., and R.G. Kelly, Processes contributing to the stifling and arrest of localized corrosion. In: Scientific Basis for Nuclear Waste Management XXX, D.S. Dunn, C. Poinssot, and B. Begg, eds., Mater. Res. Soc. Symp. Proc. 985, Paper 0985-NN08-01, Warrendale, PA, 2007.

Modeling and Measurement of Current Distribution for Localized Corrosion in Thin Layers of Particulates and Electrolyte Films

Uziel Landau, Arun Agarwal, Xi Shan, and Joe H. Payer
Case Western Reserve University

Research Objectives

The objective is to model the current patterns and distribution in thin layers of moisture and layers of moist particulates and deposits on metal surfaces. Of particular interest is the flow of current representative of corrosion scenarios at the metal surface: pitting, crevice corrosion, stress corrosion cracking, and galvanic action. Layer thicknesses range from monolayer coverage to thicker particulate layers. Results provide important insights for cathodic stifling processes, effects of surface roughness and particulates within a crevice, and the evolution of surface profiles from crevice-corrosion damage.

Approach

The project examines geometric effects, saturated and unsaturated particulate layers, chemical composition of moisture and particulates, temperature, and relative humidity. A less complex representation that is amenable to straightforward treatment was developed for the crevice-corrosion system depicted in Figure 1(a). The heterogeneous, particulate-containing film was represented in terms of a simplified equivalent system with smooth surfaces and homogeneous electrolytes, as shown in Figure 1(b). The ohmic effects due to surface irregularities and the presence of particles were accounted for by specific treatments based on system properties.

Accomplishments

External Cathode

The presence of particulates in thin electrolyte films covering the freely exposed external metal surface could significantly reduce the ability of the cathode to support metal dissolution under the crevice former, by increasing the ohmic potential drop between the cathode and the internal anode. This effect was quantified by representing the heterogeneous electrolyte in terms of a homogeneous electrolyte, accounting for the particles' effects through two corrections; (1) an effective conductivity (K_{eff}) of an equivalent homogeneous electrolyte was defined based on the volume fraction occupied by particles (ϕ_p) using Bruggeman's equation:

$$K_{eff} = K(1 - \phi_p)^{3/2}$$

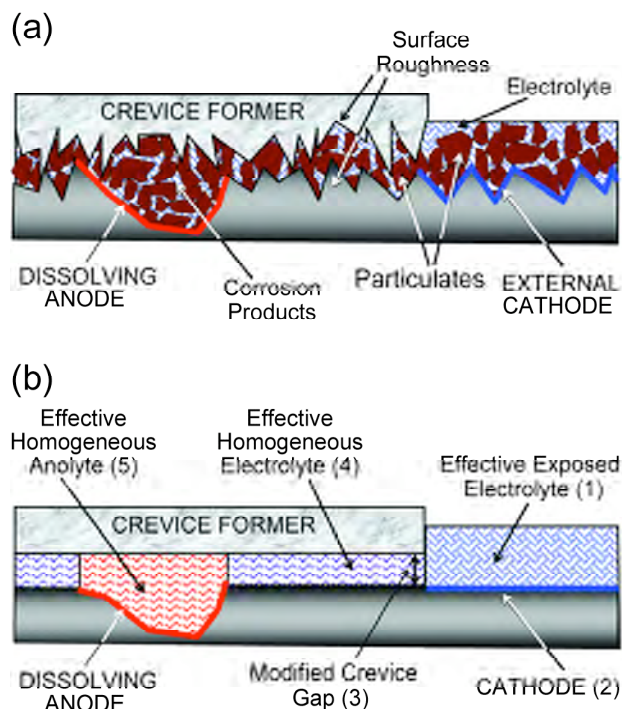


Figure 1. (a) Schematic diagram of a crevice-corrosion system indicating the various elements (particulates and surface roughness) contributing to ohmic limitations; (b) equivalent "simplified" crevice-corrosion system with (1) exposed electrolyte conductivity modified to account for the particulates on the cathode, (2) cathode kinetics adjusted for area coverage by particles; (3) equivalent smooth crevice gap obtained by constriction factor analysis for surface roughness; (4) equivalent conductivity for particles under crevice former, and (5) effective conductivity of the anolyte at the dissolution site for solid corrosion products.

and (2) the effect of the surface area coverage by the inert particles was accounted for by applying a modified kinetics parameter (exchange current density, i_0') based on total (A_T) and exposed (A_E) electrode area:

$$i_0' = i_0 \times A_E/A_T$$

Cathode current capacities (maximum current the cathode can produce) for the heterogeneous systems where current and potential fields are numerically simulated in particle-containing electrolyte were found to be in good agreement (less than 5% variation) with those obtained for homogeneous electrolytes, with corrections for the particles effects, as depicted in Figure 2. Particles with varying shapes and

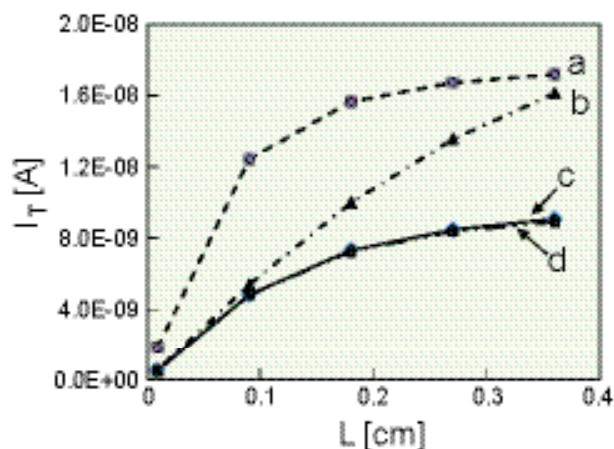


Figure 2. Effect of the cathode length (L) on the total current capacities (I_T) for the various particle effect models: (a) homogenous electrolyte corrected only for the solution conductivity, (b) homogenous electrolyte corrected only for the area coverage effect, (c) complete 3-D simulations of particulate layer (dashed line), (d) simulation of an equivalent homogenous electrolyte applying corrections for the solution conductivity and area coverage effects (solid line). Clearly, the equivalent presentation with both corrections provides excellent agreement with the detailed 3-D simulation.

arrangement, including multilayers, were analyzed, and the results corroborated the above findings. Effects of particles on cathode capacity and saturation length (no appreciable increase in capacity beyond this length) were also modeled.

Within the Crevice

The volume blockage effect of particles under the crevice former could be due to dust deposition, precipitation of deposits, and solid corrosion products. This effect was modeled by applying an effective conductivity using Bruggeman's equation (Equation 1). The resulting potential drop was found to be in agreement with the heterogeneous electrolyte (particulate-containing) model.

The surface roughness associated with the crevice former and the metal substrate is expected to form constrictions along the narrow passages, leading to high localized ohmic drop. In order to model this effect, the crevice was represented in terms of an equivalent "idealized" smooth crevice by calculating a constriction factor based on the cross-sectional gap profile. A comparison of the constriction factor correction to a full 3-D numerical simulation indicated the validity of the approach over a broad range of parameters. The effect of solid corrosion product accumulation on corrosion propagation at the dissolution site under the crevice former was modeled by decreasing the

local conductivity, based on the volume fraction occupied by the particles. As damage evolves, the volume of accumulated solid oxides resulting from metal dissolution increases and the local conductivity, K_{eff} decreases. The subsequent corrosion profiles were observed to propagate the damage evolution preferentially towards the crevice mouth (Figure 3). This effect was not seen in the system modeled without particulate accumulation. In the latter, a symmetrical cylinder-like propagation was observed at the corroding site.

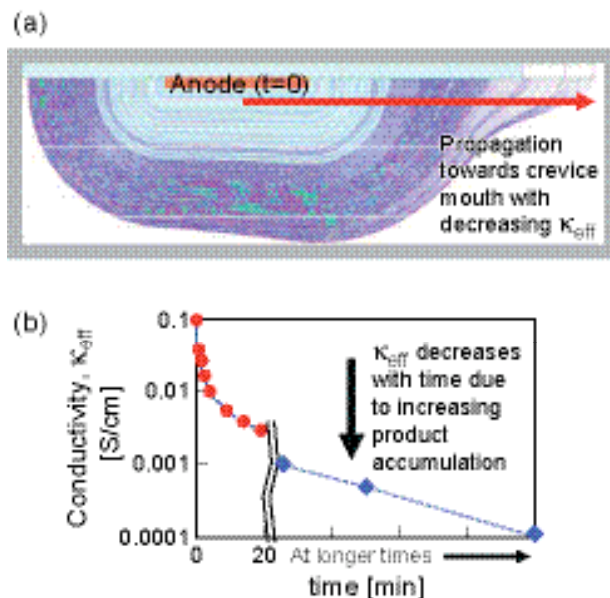


Figure 3. (a) Corrosion profile evolution in the presence of solid oxide accumulation. (b) Effective conductivity (K_{eff}) at corrosion site based on accumulated particle volume as a function of time.

Analytical Modeling

One-dimensional analytical models were developed for determining the current distribution along the cathode and for the cathode capacity in the thin electrolyte films. These models were found to be in excellent agreement with numerical results for cathodic polarization kinetics. The analysis provides scaling parameters, such as the Wagner number, for predicting the current distribution non-uniformity as a function of process parameters.

This work quantifies the ohmic effects imposed by geometrical features associated with crevices formed in thin electrolyte films, including particulates. It also determines the conditions where corrosion is limited or completely stifled due to constraints on the cathodic currents necessary to support localized corrosion.

Microelectronic and MEMS Devices for Solution Properties and Corrosion Evaluations

Chung-Chiun Liu, Meijun Shao, and Laurie Dudik
Case Western Reserve University

Research Objectives

This research focuses on the design and fabrication of microsensors to assess critical environmental parameters that can affect the corrosion of metal covered by a thin layer of particulates. The important parameters include temperature, pH, solution conductivity, oxidizing potential, and oxygen concentration. The results of this research will provide a better understanding of how these environmental parameters affect the corrosion of metal covered by a thin layer of particulates.

One of the important objectives is to experimentally obtain the needed information for establishing the diffusion coefficient of dissolved oxygen in the presence of a thin sand or other particulate layer. Knowing the diffusion coefficient of dissolved oxygen in the presence of a thin particulate layer will be useful for assessing the potential corrosion in thin layers of electrolytes and in electrolyte with particulates.

Approach

Microfabrication processing is used for the production of these sensors. Both thick film and thin film metallization techniques are used in the fabrication of the sensor prototypes. All of these sensors are operated in the electrochemical mode, even though the reaction mechanisms are different in each. For example, the solid state Pd/PdO pH sensor is operated in a potentiometric mode, whereas the oxygen sensor is operated in an amperometric mode. For conductivity measurement, high frequency (1000 Hz) alternating current is used, avoiding any potential effect on the solution.

Accomplishments

Microfabrication processing was successfully conducted to produce the microsensors. A thin film metallization technique was used to fabricate the conductivity microsensors; thick film technique was used to produce the other environmental sensors. A silicon substrate was employed for the thin film microsensors, whereas an alumina substrate was employed for the thick film microsensors. For the conductivity sensor, various dimensions of electrode width,

electrode length, tip width, and gap width were used. A general statement can be made about the results of the conductivity study: At a fixed electrode distance, the resistance decreased as the depth of the testing solution increased at a lower frequency range. At a high frequency (i.e., 10,000 Hz or higher), the solution depth showed no appreciable effect on the resistance. Thus, in our study, a frequency of 1,000 Hz was used successfully.

The present work focused on the modifications of the thick film pH and oxygen sensor. Experimental measurements of pH and dissolved oxygen concentrations in the testing solution in the presence of a sand layer were carried out.

Palladium/palladium oxide pH sensors have two versions, one a three-electrode configuration and the other a two-electrode configuration. We found the potentiometric mode of operation to perform reasonably well. Figure 1 shows one version of different sizes of the pH sensor prototypes. The electrode elements and the insulation layer are all printed by thick film processing using appropriate metallic and insulation inks, a highly cost-effective process. A very good linear relationship exists between the output of the micro-pH sensor and the pH value of the testing medium. It is important to recognize that the increase or decrease in thickness of the sand layer in the

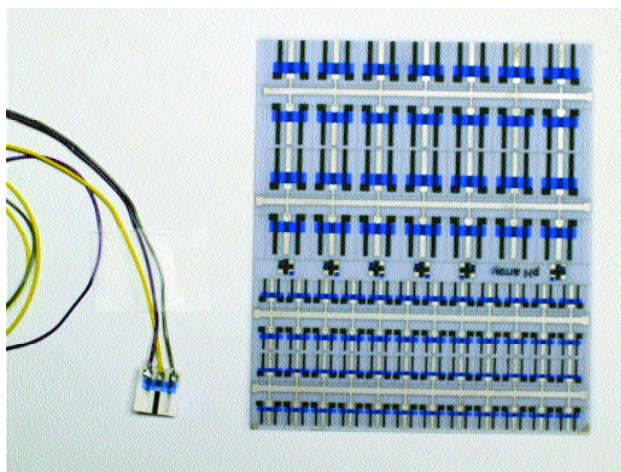


Figure 1. Thick film screen pH sensor prototypes.

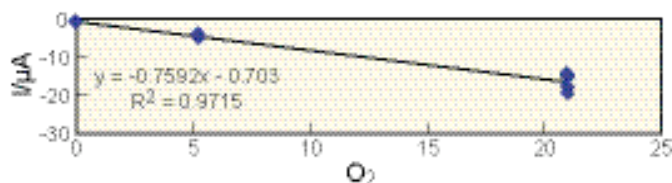


Figure 2. Performance of the oxygen sensor over a concentration range of 0 to 21% V/V.

testing solution does not affect the pH value of the testing medium. The results obtained in the pH measurements, and the approach of using thick film screen-printing technology for manufacturing this micro-pH sensor, indicate that this micro-pH sensor can be used effectively for environmental or corrosion-of-metal assessment in the presence of various sand (or similar material) layer thicknesses.

The fabricated oxygen sensor had a three-electrode configuration. Both the working and the counter electrodes are gold with the reference electrode Ag/AgCl. Thick film screen-printing processes were used to produce the sensor prototype, on an alumina substrate. The sensor was operated in the amperometric mode, and a reduction potential of -0.6 V versus the Ag/AgCl electrode was applied. The reduction current of oxygen was then used to quantify the oxygen concentration. In the experimental measurements, a 0.01M KCl was used as the testing medium, with an oxygen concentration range of 0 to 21% V/V. The sand layer thickness varied from 3 to 10 mm. Four oxygen sensors were tested each time. Figure 2 shows the relationship between the typical reduction current and the oxygen concentration.

To evaluate the diffusion coefficient of the dissolved oxygen in the sand layer, the established Cottrell equation is used:

$$I = nFAC_0\sqrt{\frac{D}{\pi t}}$$

in which n is the number of electron transfer (4 in this case), F is the Faraday constant, A is the surface area of the working electrode, which is 0.015 cm^2 , and C_0 used is $.281 \times 10^{-6} \text{ mol/cm}^3$ at 21°C . The current I was then measured as a function of time. The diffusion coefficient is calculated.

The oxygen diffusion coefficient in an aqueous solution is reported in the literature as $20 \times 10^{-6} \text{ cm}^2/\text{sec}$. In our studies, the experimental results showed that the oxygen diffusion coefficient at 21°C was $9.5 \times 10^{-6} \text{ cm}^2/\text{sec}$ and $3.1 \times 10^{-6} \text{ cm}^2/\text{sec}$ for a thickness of sand or similar particulate layer of 3 mm and 10 mm, respectively. These results are reasonable and are useful for this study.

Microsensor development and measurement of dissolved oxygen within the testing medium, in the presence of various sand-layer thicknesses, is important. As stated previously, evaluating the diffusion coefficient of dissolved oxygen in the presence of a sand or particulate layer is a major objective of this research endeavor. The result of this study will add to our knowledge about the role of dissolved oxygen in the corrosion of metal covered with a thin layer of particulates.



Optical Probes and Sensors to Determine Concentration Distributions in Thin Films on Reactive Surfaces

William H. Smyrl and Francis Guillaume
University of Minnesota

Research Objectives

The objective was to reveal the reaction distributions on heterogeneous, reactive metal surfaces. Previous work has revealed the current/potential distributions at individual reactive sites and at arrays of sites that may be galvanically coupled on metal surfaces, including those under thin films of electrolytes. Fluorescence techniques are powerful tools to measure physico-chemical conditions (pH, gas concentration) and anolyte species *in situ*. These have been adapted in previous work in our laboratory to monitor localized corrosion on aluminum alloys with a submicrometric spatial resolution. The goal in the present study has been to design fluorescent multiprobe sensors capable of monitoring oxygen partial pressure, pH, and specific metal ions at and near reactive (corroding) surfaces. In addition, there has been interest in extending the studies to reaction and concentration distributions at metal surfaces under particulate layers.

Approach

The fluorescent sensor probes were based on isolating the probes in matrix hosts to prevent dissolution of the dyes in the aqueous electrolytes. The matrix host must fulfill several criteria that include: (1) optical transparency to facilitate measurements without interference due to inherent fluorescence from the matrix; (2) solubility of the dye(s) in the matrix; (3) matrix must not quench the dye fluorescence; (4) matrix must be permeable to oxygen, to H⁺ ions, or to metal cations; (5) sensor must not consume the species to be sensed; (6) sensor must be reversible, and; (7) the immobilized dye must not leach out from the matrix. It was discovered that these criteria were difficult to satisfy.

Accomplishments

Oxygen Sensor Results

A miniature optical sensor was developed and has been shown to measure oxygen in the gas and liquid phases.

It utilizes the fluorescence of a ruthenium dye immobilized in a poly(dimethylsiloxane)(PDMS) matrix for sensing. The fluorescence is quenched in the presence of oxygen, but oxygen is not consumed in the process. The techniques for assembly and for operation of the sensor were developed. Future developments may include oxygen depletion in crevice corrosion and other localized corrosion processes. Further miniaturization may enable one to use the sensor on a scanning fiber to image the concentration field of oxygen around reactive sites on a metal immersed in solution.

pH Sensor Results

The fluorescence intensity versus pH was measured for a derivatized optical fiber (DOF) immersed in solution. A 470 nm Panasonic blue light emitting diode (LED) was used as the excitation source. The sensor response time was not measured, but appeared to be extremely fast (<1 second). The fluorescence characteristics were similar to those found for the dye dissolved in aqueous solution. It was discovered that the intensity at the end points of pH 2 and pH 10 are too high. This was due to dye leakage from the polymerized acrylamide gel matrix. Results were obtained with an improved dual fiber configuration consisting of a single-mode fiber coupled to an Ar ion laser as illumination and a DOF multimode fiber for sensing. The two fibers were assembled side-by-side in a glass capillary, embedded in epoxy, polished at the end, and treated as above to form the photo-polymerized acrylamide host plus dye on the multimode fiber. The dual fiber configuration gave useful spectra with virtually no distortion of the fluorescein spectrum. This new configuration was adopted for experiments for pH sensing. Then the photo-polymerization of acrylamide gels was adopted to formation of thin films for pH sensing/monitoring. Dye leakage from the polymerized matrix was not solved by modifying the photo-polymerization solution. The leakage caused hysteresis and the termination of the approach. Several approaches for pH sensor development were studied. None was completely successful.

This page intentionally left blank.

High-Temperature Multi-Species Solution Properties and Behavior

David R. Cole¹, Lawrence N. Anovitz^{1,2}, Miroslaw S. Gruszkiewicz¹, Donald A. Palmer¹, Jorgen Rosenqvist¹, David J. Wesolowski¹, Leslie L. Wilson¹, Andre Anderko³, George Engelhardt³, Peming Wang³, and Digby D. Macdonald⁴

¹Oak Ridge National Laboratory (ORNL) | ²University of Tennessee | ³OLI Systems Inc. | ⁴Pennsylvania State University

Project Objectives

This project is aimed at developing an enhanced scientific understanding of the behavior of high-temperature, multi-species solutions. Earlier in the reporting period, the goals were to complete the study of the partitioning of mineral acids from liquid water to steam as a function of temperature, and the scoping study of the effect of tuff particles on brine chemistry. Some of these earlier results were transmitted to OLI Systems for use in their chemical modeling subtask in order to enhance our understanding of the corrosion evolutionary path of a metal alloy–aqueous system. More recently, we have initiated an effort to determine the solution chemistry associated with actively corroding crevices, in particular, the speciation of W, Mo, and Cr in concentrated brines relevant to the localized crevice environment.

Approach

The approach in this phase of the project was to take advantage of unique experimental techniques developed at ORNL: (1) to use a high temperature volatility apparatus to quantify liquid/vapor interactions as a function of temperature, solution composition, prevailing humidity, and time; (2) to use high temperature *in situ* pH cells to determine the pH of brines interacting with volcanic tuff as a function of temperature, solution composition, and time; and (3) to incorporate the experimental results into a Mixed-Solvent Electrolyte (MSE) computer model database to enhance our understanding of the corrosion evolutionary path of the system. A new subtask focuses on using spectroscopic and *in situ* pH methods to determine the speciation and thermodynamic stability of metal ions found in active crevices on alloy surfaces as a function of temperature, solution composition, and acidity.

Accomplishments

Partitioning of Anions from the Liquid Film to the Vapor Phase

Experiments were completed utilizing the ORNL volatility apparatus to determine the partitioning constants of the inorganic acids of fluoride, nitrate, chloride, and bisulfate over the temperature range of 60 to 200°C. The liquid

phase was composed of sodium salts of acids, with the pH of the solution being controlled by the acid dissociation constant of bisulfate that is known from published results from our laboratory (Dickson et al., 1990). Knowledge of pH is critical, as it dictates the concentrations of these acids in the liquid phase that are known to be many orders of magnitude more volatile than their corresponding sodium salts. The results have been obtained using a crude activity coefficient model at this time until OLI Systems can process the data to derive accurate coefficients. The approximate order of volatility for these acids is $\text{HF} \gg \text{HNO}_3 > \text{HCl} > \text{H}_2\text{SO}_4$. Indeed, this initial treatment of the data did not include the association of the relatively weak acid, HF, and this correction will only enhance the partitioning constant further.

The implications of these results are that in an open system, fluoride will readily be lost to the air from solution, and this effect will also tend to raise the pH of the remaining solution as HF is lost. Secondly, nitrate is more volatile than chloride by about a factor of two over the range of temperatures investigated here, noting that the partitioning constants of all electrolytes increase dramatically as the critical temperature of water is approached. Finally, sulfate will only partition significantly from a liquid film to the surroundings at low pH and may be considered to be less volatile at all conditions than the other three mineral acids.

Solution Chemistry Associated with the Interaction of Tuff Particles with Brine

Batches of well-characterized volcanic tuff powders were reacted with NaCl brines at 0.1 and 1.0 molal ionic strength and a starting $\text{pH}_m \{ \equiv -\log(\text{mH}^+) \}$ ranging from 1 to 3 at 80–120°C for periods up to two weeks. Figure 1 is a representative plot, showing that the powdered tuff (surface area 3.5 m²/g) is able to increase the pH of the solution significantly over relatively short time periods (days). Comparison of the X-ray diffraction patterns of the starting material and run products indicates the formation of the clay mineral montmorillonite during the reaction with abundant alkali feldspar in the tuff with the acidic brine. These preliminary experiments demonstrate that the tuff itself has a significant capacity to rapidly neutralize acidic solutions that might be encountered on a tuff-dust-covered metal surface at elevated temperatures.

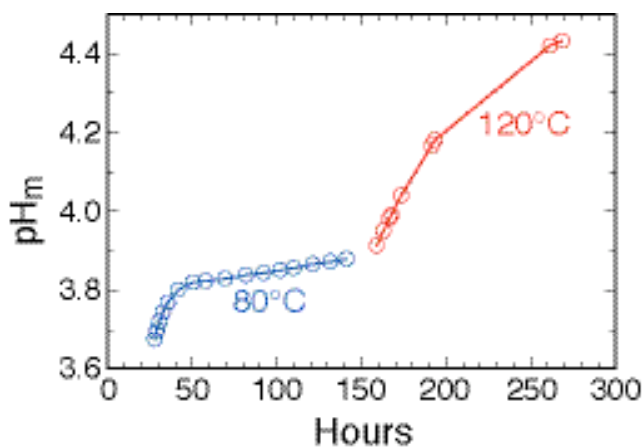


Figure 1. Plot of measured pH_m for a 41.5 grams of a starting aqueous solution of $\text{pH}_m = 3.0$ and ionic strength 1.0 molal (NaCl) reacted with 1.07 grams of tuff sample as a function of time in the stirred hydrogen-electrode cell.

Solution Chemistry Associated with an Actively Corroding Crevice

This new task was initiated to obtain thermodynamic data on the interaction of specific metal ions (i.e., Cr(III), Ni(II), Fe(II), Mo(V,VI) and W(VI)) with highly acidic chloride and nitrate brines to 120°C. We currently have been investigating the speciation of W(VI) at elevated temperatures. A number of potentiometric titrations of Na_2WO_4 solutions at 50°C in 5.0 molal NaNO_3 ionic medium have been performed using an automatic titrator (Figure 2). The value "n" in the figure is defined as the total number of 'missing' protons (i.e., the difference between the concentration of H^+ calculated from the input solution compositions and the measured H^+ concentration) divided by the total metal concentration in solution at each titration point. The steep slopes of the curves in the pH-range 5.5–6.5

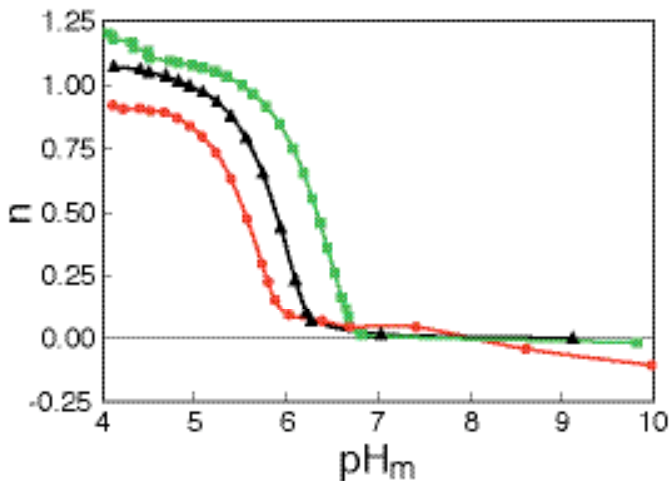


Figure 2. Proton uptake by WO_4 versus pH_m is defined as the average number of protons per WO_4 unit. Green squares = 0.003 molal total WO_4 . Black triangles = 0.001 molal total WO_4 . Red circles = 0.0003 molal total WO_4 .

indicate formation of polynuclear species. The relatively large shift of the curves to lower pH with decreasing total WO_4 concentration and the noninteger values of the plateaus below pH 5 also suggest that the solution speciation is dominated by larger polynuclear species. The identity of these polynuclear species is being assessed by a combination of an ultraviolet/visible information system (UV/VIS) and Raman spectroscopy.

Related Publications

Dickson, A.G., D.J. Wesolowski, D.A. Palmer, and R.E. Mesmer, Dissociation constant of bisulfate ion in aqueous sodium chloride solutions to 250°C. *J. Phys. Chem.*, 94, 7978–7985, 1990.

This page intentionally left blank.